



## Article

# Evaluation of Three Air Temperature Reanalysis Datasets in the Alpine Region of the Qinghai–Tibet Plateau

Xiaolong Huang<sup>1,2</sup>, Shuai Han<sup>3,\*</sup>  and Chunxiang Shi<sup>3</sup>

<sup>1</sup> Heavy Rain and Drought-Flood Disasters in Plateau and Basin Key Laboratory of Sichuan Province, Chengdu 610072, China

<sup>2</sup> Sichuan Meteorological Observation and Data Centre, Chengdu 610072, China

<sup>3</sup> National Meteorological Information Center, China Meteorological Administration, Beijing 100081, China

\* Correspondence: hans@cma.gov.cn; Tel.: +86-177-1026-2113

**Abstract:** Surface air temperature is a critical element in the surface–atmosphere interaction, energy exchange, and water cycle. Multi-source fusion reanalysis products (hereafter referred to as reanalysis) have spatiotemporal continuity and broad applicability that can provide key data support for various studies such as glacier melting, soil freeze-thaw and desertification, ecosystem, and climate change in the alpine region of the Qinghai–Tibet Plateau (QTP). Surface air temperature observations collected at 17 weather stations in the High-cold region Observation and Research Network for Land Surface Process and Environment of China (HORN) over the period of 2017–2018 are implemented to evaluate the advanced and widely used surface air temperature reanalysis datasets, which include the European Centre for Medium-Range Weather Forecasts (ECMWF) Fifth Generation Land Surface Reanalysis (ERA5L), the U.S. Global Land Data Assimilation System (GLDAS), and China Meteorological Administration Land Data Assimilation System (CLDAS). Results are as follows: (1) Evaluation results of temporal changes and spatial distribution characteristics indicate that the three reanalysis datasets are consistent with in-situ observations in the alpine region of the QTP. CLDAS is more consistent with observations and can better describe details of temperature distribution and variation than ERA5L and GLDAS. (2) For the evaluation period, CLDAS is 0.53 °C higher than the in-situ observation, while ERA5L and GLDAS are lower than the in-situ observation by −3.45 °C and −1.40 °C, respectively. (3) The accuracy of CLDAS is better than ERA5L and GLDAS under different elevations and land covers. We resampled three reanalysis datasets with a spatial resolution of 0.25° and used the two most common interpolation methods to analyze the impact of spatial resolution and different interpolation methods on the evaluation results. We found that the impact is small. In summary, the three reanalysis datasets all have certain applicability in the alpine region of the QTP, and the accuracy of CLDAS is significantly higher than ERA5L and GLDAS. The results of the present paper have important implications for the selection of reanalysis data in the studies of climate, ecosystem, and sustainable development in the QTP.

**Keywords:** air temperature; Qinghai–Tibet Plateau; reanalysis dataset; alpine region; applicability



**Citation:** Huang, X.; Han, S.; Shi, C. Evaluation of Three Air Temperature Reanalysis Datasets in the Alpine Region of the Qinghai–Tibet Plateau. *Remote Sens.* **2022**, *14*, 4447. <https://doi.org/10.3390/rs14184447>

Academic Editors: Massimo Menenti, Yaoming Ma, Li Jia and Lei Zhong

Received: 11 July 2022

Accepted: 1 September 2022

Published: 6 September 2022

**Publisher's Note:** MDPI stays neutral with regard to jurisdictional claims in published maps and institutional affiliations.



**Copyright:** © 2022 by the authors. Licensee MDPI, Basel, Switzerland. This article is an open access article distributed under the terms and conditions of the Creative Commons Attribution (CC BY) license (<https://creativecommons.org/licenses/by/4.0/>).

## 1. Introduction

The Qinghai–Tibet Plateau (QTP) is regarded as the Earth's “Third Pole” and “Asian Water Tower” [1,2]. It is the highest plateau in the world with an average elevation of over 4000 m. The strong dynamic and thermodynamic effects [3] of the QTP significantly affect atmospheric circulations in the northern hemisphere, as well as the Asian monsoon process and the climate patterns in East Asia [4,5], and have extremely important impacts on global climate change [1–14]. Glaciers, frozen soil, meadows, snow, and wetlands are widely distributed in the alpine region of the plateau, where the headwaters of China's major rivers are located. The alpine region of the plateau is an important area of ecological barrier, but it is also an area of harsh climatic conditions [6] and fragile ecological environments [9]

with low levels of economic development [5]. Climate change in the QTP and the various impacts it brings have become a frontier and hotspot in earth system science research, which has attracted extensive attention within the scientific community [1,2,14]. Surface air temperature is a key variable in the land-surface-atmosphere interaction and energy exchange, as well as in water cycle processes. It is also an important basis [7,8] for the studies of glacial melting, soil freeze-thaw and desertification, and ecosystems and climate change in the plateau. Due to the vast area of the QTP, the restrictions of transport, and the terrain environment, weather stations are only sparsely distributed in the QTP and mainly concentrated in the eastern and southern parts of the QTP [15]; few stations are located in the western and northern parts of the plateau [16]. To complicate matters further, many stations in the QTP are established late and with short sequences of observations, which makes the temperature observations unable to fully reflect the state of the surface air temperature over the entire plateau. Therefore, reanalysis products of temperatures with spatiotemporal continuity and broad applicability are required to provide critical data support [15–19] for climate change and impact studies over the QTP [20,21].

In recent years, several research institutions in the United States, the European Union, China, Japan, and other countries have successfully developed a series of land surface reanalysis systems and multi-source data fusion analysis systems [22–24]. Great progress has been made in the land surface reanalysis dataset. Compared with atmospheric reanalysis datasets, land surface reanalysis products have higher spatiotemporal resolutions and wider application. At present, the most advanced land surface reanalysis datasets include the ECMWF Fifth Generation Land Surface Reanalysis (ERA5L) [25–30], the NASA Global Land Data Assimilation System (GLDAS) [31–33], and the China Meteorological Administration Land Surface Data Assimilation System (CLDAS) [34–38]. These datasets include surface meteorological elements and soil information. A series of research results have been achieved based on the application of these datasets in studies of weather and climate prediction, water resources management and water cycle, etc.

Due to differences in input data, numerical assimilation models, parameterization schemes, and the spatiotemporal resolutions of final products, these reanalysis datasets demonstrate quite different performances in different regions. Therefore, accuracy evaluation and applicability analysis of various reanalysis datasets are a prerequisite for their application. Several studies have evaluated the applicability of CLDAS, ERA5L, and GLDAS in the QTP [39–42]. For example, Han et al. [40] compared surface air temperature from CLDAS and GLDAS with observations collected at 2380 weather stations in China over the period 2010–2015. Their results indicate that surface air temperatures in the two reanalysis datasets are lower than observations in the QTP, while the accuracy and correlation of CLDAS with station observations are better than GLDAS. On different temporal and spatial scales, Huang et al. [41] verified CLDAS, ERA5L, and GLDAS against observations collected at 2265 weather stations in China during 2017–2019. They found that the three aforementioned reanalysis datasets can represent the characteristic temperature changes in the QTP well, although they are lower than observations. CLDAS is highly consistent with station observations, and its accuracy is significantly better than the other two reanalysis datasets. GLDAS is better than ERA5L. Liu et al. [42] selected 32,552 assessment stations that have been fused into the CLDAS system and 12,403 non-assessment stations that are non-fused into the CLDAS system as the data sources for evaluation and conducted dependent and independent verifications of CLDAS hourly temperature data in different regions of China. Results of both dependent and independent verification confirm that CLDAS has a relatively high accuracy and applicability in the QTP. Wang et al. [43] compared GLDAS with China's gridded surface air temperature dataset in the QTP and surrounding areas. They found that GLDAS performs better in arid regions than in sub-humid areas, and that the data are more accurate during 1979–1994 than during 2000–2007.

In summary, the three aforementioned reanalysis datasets all demonstrate a relatively high applicability in the QTP and thus have potential values for weather and climate studies. We also found that the previous applicability studies of temperature reanalysis

datasets often use observations collected at operational weather stations of the China Meteorological Administration as reference data, and, while these observations have high accuracy and reliability, the following issues need to be addressed: (1) Many national-level meteorological station observations have been included in the international exchange list, and many of the data have been used as input for assimilation and/or data fusion to produce various reanalysis datasets. Therefore, it is hard to achieve independent results using these data to verify reanalysis products. (2) Most of these weather stations are located in suburbs of cities or areas along highways that are easily accessible. Their coverage of QTP topography and landform types is limited, which makes the evaluation results have limited reference value for assessing the reliability of the reanalysis datasets in the QTP. Based on the aforementioned discussion, the present study uses in-situ observations provided by “China Alpine Region Surface Process and Environmental Monitoring Research Network” [44,45] to evaluate surface air temperature from CLDAS, ERA5L, and GLDAS. The present study reveals some important similarities and differences in comparison to previous studies. Results of the study will be helpful in studies of the special atmospheric, hydrological, and ecological processes in the alpine region of the QTP [46].

## 2. Data and Methods

### 2.1. Data

#### 2.1.1. Reanalysis of Surface Air Temperature

##### 1. CLDAS dataset

CLDAS is a land-surface data assimilation system developed in the National Meteorological Information Center of the China Meteorological Administration (CMA) [22,35]. Advanced fusion technology is combined with independent innovations proposed in CMA during the development of CLDAS. Multi-grid variational analysis, spatial grid stitching, discrete ordinate shortwave radiation remote sensing retrievals, terrain correction, ensemble simulations of multiple land surface models (CLM, Noah-MP, CoLM), etc., are combined to produce surface pressure, ground precipitation, temperature, humidity, UV winds, shortwave radiation, surface air temperature and humidity, soil moisture and temperature, etc. The China Land-surface Data Assimilation System Version 2 (CLDAS-V2.0) [22] was released in 2015 and upgraded in 2018. This system can efficiently fuse observations collected at nearly 60,000 weather stations in China with numerical prediction data and satellite remote sensing data, and can release a real-time fused land surface data analysis product on  $0.05^\circ \times 0.05^\circ$  grids at 1 h intervals. This product has been widely applied in meteorological and agricultural studies [36,37,41].

##### 2. ERA5L dataset

ERA5L is a high spatiotemporal resolution global land surface reanalysis dataset produced by ECMWF for global land areas. It is a component of the fifth-generation European Reanalysis Product (ERA5) [28] that was developed within the framework of the European Commission Copernicus Climate Change Service (C3S). Based on outputs of numerical simulations of the ECMWF land-surface model, ERA5L is a downscaled dataset from the ERA5 climate reanalysis, and elevation correction for near-surface thermal states is conducted to ensure consistent evolution of water and energy cycles over the land [27]. ERA5L can be applied for trend and anomaly analysis. ECMWF released the ERA5L product in 2019, which contains data from 1981 until present, with ongoing updates. The historical dataset over 1950–1980 was released in September 2021. With a high spatial resolution of  $0.1^\circ \times 0.1^\circ$  and temporal resolution of 1h, as well as long data sequences and data consistency, ERA5L provides a strong support in hydrological study and numerical weather/climate model initialization. It is also widely applied in studies of water resources and land and environment management [29,30,47], etc.

##### 3. GLDAS dataset

GLDAS is produced by the NASA Goddard Space Flight Center (GSFC) and the National Centers for Environmental Prediction (NCEP) of National Oceanic and Atmospheric

Administration (NOAA). Surface observations and satellite remote sensing retrievals are assimilated into the land surface models of Noah, Mosaic, CLM, and VOC to simulate global surface variables [32] (such as soil moisture, land surface temperature, etc.) and fluxes (such as evaporation, sensible heat flux, etc.). GLDAS has been widely applied to global climate change studies and comparative studies with other remote sensing products. GLDAS provides two versions of the dataset (GLDAS-1 [48] and GLDAS-2 [49]). The present study uses GLDAS-2, and the spatial and temporal resolutions of the dataset are 1h and 0.25°, respectively.

Table 1 lists the attributes of the datasets evaluated in the present study, including their spatial and temporal resolutions, coverages, and data download sources.

**Table 1.** Characteristics of the reanalysis temperature datasets.

Dataset	Areal Coverage	Spatial Resolution	Temporal Resolution	Unit	Website for Download
GLDAS	180°W–180°E; 60°S–90°N	0.25° × 0.25°	3 hourly	K	<a href="http://disc.sci.gsfc.nasa.gov/hydrology/data-holdings">http://disc.sci.gsfc.nasa.gov/hydrology/data-holdings</a> (accessed on 30 June 2022)
ERA5L	180°W–180°E; 60°S–90°N	0.1° × 0.1°	Hourly	K	<a href="https://cds.climate.copernicus.eu/cdsapp#!/dataset/reanalysis-ERA5L?tab=form">https://cds.climate.copernicus.eu/cdsapp#!/dataset/reanalysis-ERA5L?tab=form</a> (accessed on 30 June 2022)
CLDAS	70°E–140°E; 0°–60°N	0.05° × 0.05°	Hourly	K	<a href="http://data.cma.cn/">http://data.cma.cn/</a> (accessed on 30 June 2022)

### 2.1.2. In-Situ Temperature Observations in the Alpine Region of the QTP

The in-situ temperature observations used to evaluate the reanalysis datasets are provided by the Tibetan Plateau Data Center of China. The data were downloaded from <http://data.tpdc.ac.cn/> (accessed on 3 January 2022). These observations are collected at 17 field observation sites (Figure 1), which are evenly distributed in the alpine region of the QTP. Temperature, precipitation, wind speed and wind direction, relative humidity, radiation, evaporation, etc., are measured. Long-term surface processes and environmental changes are continuously monitored to understand patterns of climate and water resource changes in the headwater areas of the Yangzi River and the Yellow River. This information will be helpful to reveal the changes in ecosystem structure and function, build ecological protection barriers, and grasp the mechanism for the occurrence of natural disasters such as ice and snow freezing and thawing [44]. All the in-situ temperature observations used in the present study are daily mean temperature. Table 2 lists the properties of the in-situ observation sites and related information [45].

### 2.2. Methods

To quantitatively compare the consistency of the three reanalysis datasets with in-situ observations and evaluate their errors of daily average temperatures, the reanalysis data from 2017–2018 are divided into eight times per day (00, 03, 06, 09, 11, 14, 17, 20 UTC), which is the division used in GLDAS. The arithmetic mean is taken as daily mean temperature for individual reanalysis datasets. Based on the latitude and longitude information of the observation sites, daily mean temperatures from reanalysis are interpolated to the observation sites using the nearest neighbor interpolation method. Two sequences of daily temperatures from the reanalysis and from the in-situ observations, with 11,635 samples in each sequence, are then compared. Pearson correlation coefficient (CC), mean bias error (MBE), root-mean-square error (RMSE), Nash–Sutcliffe efficiency coefficient (NSE) [50,51], Kling–Gupta efficiency (KGE) [52,53], and Willmott’s Index of Agreement (WIA) [54] are then calculated to evaluate the accuracy and applicability of CLDAS, ERA5L, and GLDAS

temperature data in the alpine region of the QTP. The calculations of the aforementioned indices are as follows:

$$CC = \frac{\sum_{i=1}^n (R_i - \bar{R})(S_i - \bar{S})}{\sqrt{\sum_{i=1}^n (R_i - \bar{R})^2} \sqrt{\sum_{i=1}^n (S_i - \bar{S})^2}} \quad (1)$$

$$MBE = \frac{1}{n} \sum_{i=1}^n R_i - S_i \quad (2)$$

$$RMSE = \sqrt{\frac{1}{n} \sum_{i=1}^n (R_i - S_i)^2} \quad (3)$$

$$NSE = 1 - \frac{\sum_{i=1}^n (R_i - S_i)^2}{\sum_{i=1}^n (S_i - \bar{S})^2} \quad (4)$$

$$KGE = 1 - \sqrt{(CC - 1)^2 + (\alpha - 1)^2 + (\beta - 1)^2} \text{ with } \alpha = \frac{\bar{R}}{\bar{S}}, \text{ and } \beta = \frac{\sigma_R}{\sigma_S} \quad (5)$$

$$WIA = 1 - \frac{\sum_{i=1}^n (R_i - S_i)^2}{\sum_{i=1}^n (|R_i - \bar{S}| + |S_i - \bar{S}|)^2} \quad (6)$$

where  $R_i$  is the reanalysis temperature interpolated to the observation site,  $S_i$  is the in-situ observation at the site,  $n$  is the total number of records that participate in the evaluation, and  $\bar{R}$  and  $\bar{S}$  denote the averages of reanalysis data and observations during the study period, respectively.  $CC$  (Equation (1)) represents the correlation between reanalysis and observations with values that range within  $[-1, 1]$ .  $|CC| = 1$  indicates that the two sequences are completely linearly correlated;  $CC = 0$  means there is no correlation between the two sequences, and  $0 < |CC| < 1$  indicates that there is a certain degree of linear correlation between the two. The closer  $|CC|$  is to 1, the higher the linear relationship is; the closer  $|CC|$  is to 0, the weaker the linear correlation is between the two.  $CC > 0$  indicates that the reanalysis and the in-situ observations have the same trends of change, and  $CC < 0$  means that they have opposite trends.  $MBE$  (Equation (2)) reflects the deviations of reanalysis data from observations. Negative  $MBE$  values indicates that the reanalysis data are lower than the observation, and vice versa.  $RMSE$  (Equation (3)) shows the overall difference between the reanalysis and the observations, including systematic and non-systematic biases. A closer-to-0  $RMSE$  corresponds to a more accurate reanalysis dataset.  $NSE$  (Equation (4)) is widely applied to quantify the prediction ability of hydrological models. It reflects the consistency of two datasets:  $NSE = 1$  indicates that the reanalysis data are completely consistent with the observations;  $NSE \leq 0$  indicates that the two datasets are inconsistent with each other. The  $KGE$  (Equation (5)) is based on a decomposition of the  $NSE$  into its constitutive components (correlation, mean bias, and variability bias) and is increasingly used for model calibration and evaluation.  $\sigma_R$  and  $\sigma_S$  are the standard deviations in reanalysis and in-situ observations, respectively.  $KGE$  can vary from negative infinity to 1, and  $KGE = 1$  indicates perfect agreement between simulations and observations.  $WIA$  (Equation (6)) is similar to  $NSE$ , but the denominator of the main term in the equation is the potential maximum difference [54]. The value of  $WIA$  ranges between 0 (not consistent) and 1 (perfectly consistent). On the scatterplot of reanalysis versus in-situ observations, both  $WIA$  and  $NSE$  indicate how close the data points are to the fitted 1:1 line. During the evaluation period, all samples used for evaluation are calculated based on the cumulative results of daily observations.

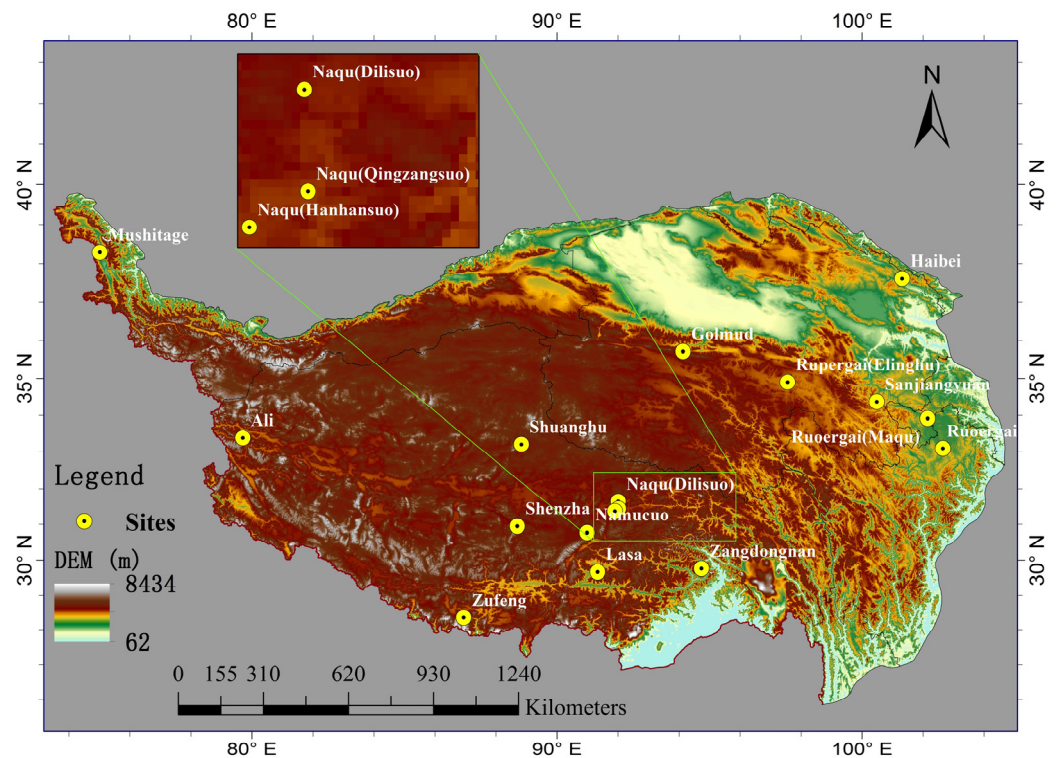


**Figure 1.** Elevation of the study area and distribution of in-situ observation sites.

**Table 2.** Properties of in-situ observation sites and related information.

NO.	Name	Longitude (°)	Latitude (°)	Elevation (m)	Height of the Sensor from the Ground (m)	Land Cover Type
1	Zangdongnan	94.7363	29.7593	3326	1.3	Grassland in forests
2	Namucuo	90.9885	30.7740	4730	1.5	Alpine meadow
3	Zufeng	86.9422	28.3590	4276	1.5	Sand and gravel
4	Golmud	94.1333	35.7167	4538	2.0	Alpine meadow
5	Lasa	91.3333	29.6667	3688	1.5	Artificial grassland
6	Mushitage	75.0183	38.2868	4400	1.5	Gravel
7	Ali	79.7013	33.3917	4264	1.5	Desert
8	Rupergai (Elinghu)	97.5588	34.9021	4278	2.0	Alpine meadow
9	Sanjiangyuan	100.4833	34.3667	3958	1.5	Alpine meadow
10	Shenzha	88.7000	30.9500	4675	2.0	Alpine meadow
11	Ruergai	102.6509	33.1026	3483	2.7	Peatland
12	Ruergai (Maqu)	102.1515	33.9205	3430	2.0	Alpine meadow
13	Naqu (Dilisu)	92.0097	31.6437	4602	1.8	Alpine meadow
14	Naqu (Qingzangsu)	92.0170	31.4410	4500	1.5	Alpine meadow
15	Shuanghu	88.8322	33.2167	4939	2.0	Alpine meadow
16	Haibei	101.3167	37.6167	3220	1.5	Alpine meadow
17	Naqu (Hanhansuo)	91.9000	31.3700	4509	1.5	Alpine meadow

Note: The properties of these sites are derived from the metadata provided in <http://data.tpdc.ac.cn> (accessed on 18 May 2022). The unit of latitude and longitude in degree, minute, and second is transferred to decimal unit in degree and keeps four decimal places. For a few sites where the metadata is missing, the properties are derived from other information. For example, the elevation at Shuanghu is derived from 90 m-resolution DEM, and the land cover type at Ali is derived from <http://www.horn.ac.cn/index.jsp> (accessed on 18 May 2022).

### 3. Results Analysis

#### 3.1. Comparative Analysis of Spatial Distribution Characteristics

Spatial distributions of average temperature for reanalysis datasets and in-situ observations during the study period of 2017–2018 are displayed in Figure 2, which clearly shows that the three reanalysis datasets and the in-situ observations roughly follow the variation of latitude and elevation. Despite the slight differences at local or regional scales, the magnitude and spatial distribution of temperature are basically the same for these datasets (Figure 2a). Temperature gradually increases from north to south, and high temperature

centers are located in southeastern Tibet, southwestern Sichuan, and northwestern Yunnan. The Qaidam Basin in the northwest of Qinghai is surrounded by mountains. The average elevation of the basin is about 2600 m, which is lower than the surrounding areas. The annual average temperatures in the three reanalysis datasets in the Qaidam Basin are all significantly higher than those of the surrounding areas. The average elevation of the Kunlun Mountains and Karakoram Mountains located in western Tibet is more than 5500 m, and the temperature is significantly lower than other areas in the same latitude. Compared to ERA5L and GLDAS, CLDAS describes more details of temperature changes with altitude. For example, CLDAS aptly describes the dramatic temperature changes caused by large altitude differences in the Hengduan Mountains region located at the junction of Tibet, Sichuan, and Yunnan, where mountains, valleys, and rivers are intertwined. In contrast, the other two reanalysis datasets can barely reflect this characteristic distribution of temperature in the Hengduan Mountains.

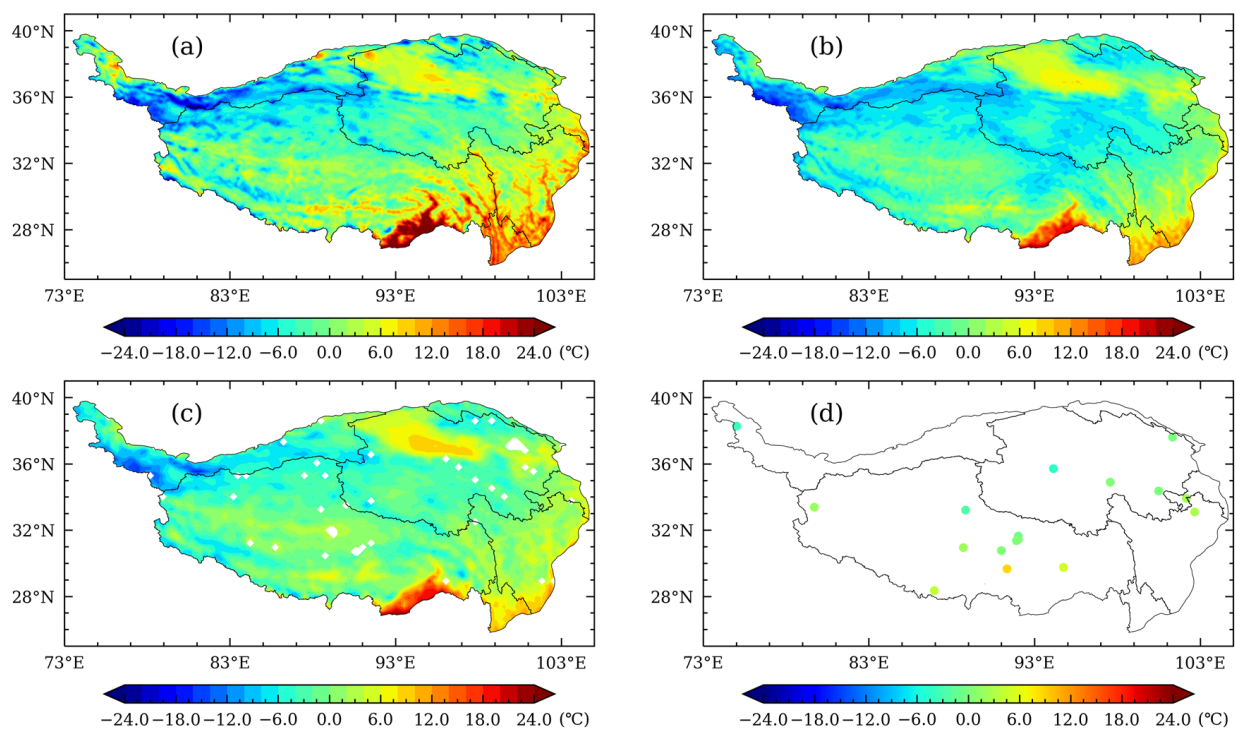


**Figure 2.** Spatial distributions of annual mean temperature over 2017–2018 ((a) CLDAS; (b) ERA5L; (c) GLDAS; (d) in-situ observations).

Spatial distributions of seasonal temperature are displayed in Figures 3–6. In the spring (Figure 3), CLDAS temperature is higher than ERA5L and GLDAS in the entire study area except the Qaidam Basin and the low-elevation region of southern Tibet, where CLDAS is lower than ERA5L and GLDAS. ERA5L and GLDAS show large differences in the spatial distribution of air temperature in the plateau area, though CLDAS has a small difference. ERA5L is also significantly lower than CLDAS and GLDAS in the central QTP. In the summer (Figure 4), the spatial distributions of CLDAS and GLDAS are similar to each other, while ERA5L is obviously lower than the other two reanalysis datasets. In the autumn (Figure 5), CLDAS and ERA5L are closer to each other, while GLDAS is lower than CLDAS and ERA5L in the high-elevation region of western QTP, but higher in the low-elevation region of the southeastern QTP. In the winter (Figure 6), spatial distributions of the three reanalysis datasets are basically consistent, although ERA5L is lower than CLDAS and GLDAS in southeastern Qinghai and northeastern Tibet. Overall, compared to GLDAS and ERA5L, CLDAS is closer to observations and demonstrates higher spatial consistency.

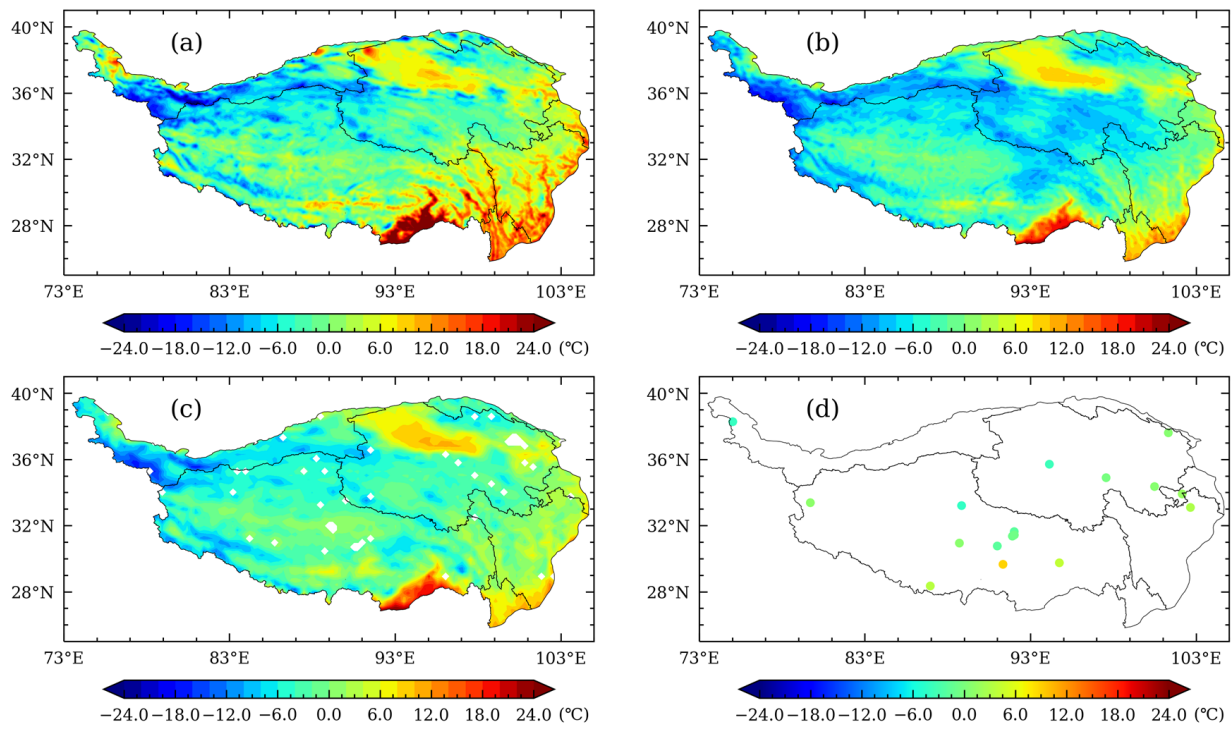


**Figure 3.** Spatial distributions of spring mean temperature over 2017–2018 ((a) CLDAS; (b) ERA5L; (c) GLDAS; (d) in-situ observations).

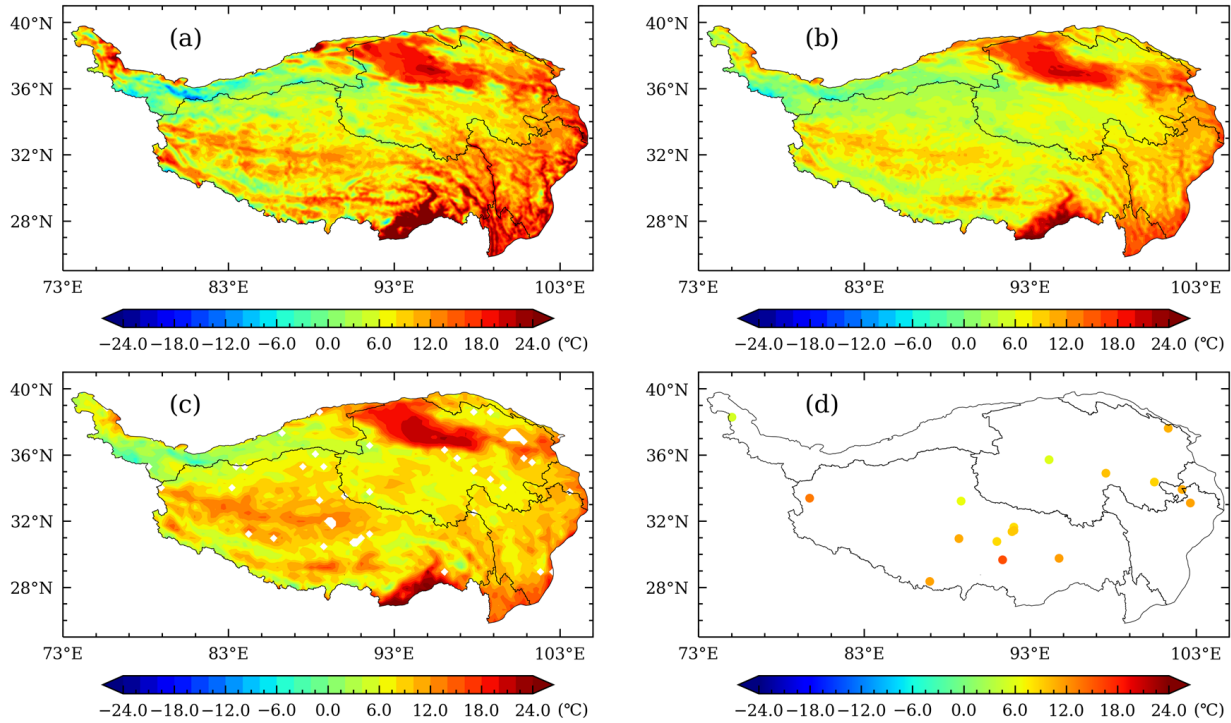


**Figure 4.** Spatial distributions of summer mean temperature over 2017–2018 ((a) CLDAS; (b) ERA5L; (c) GLDAS; (d) in-situ observations).

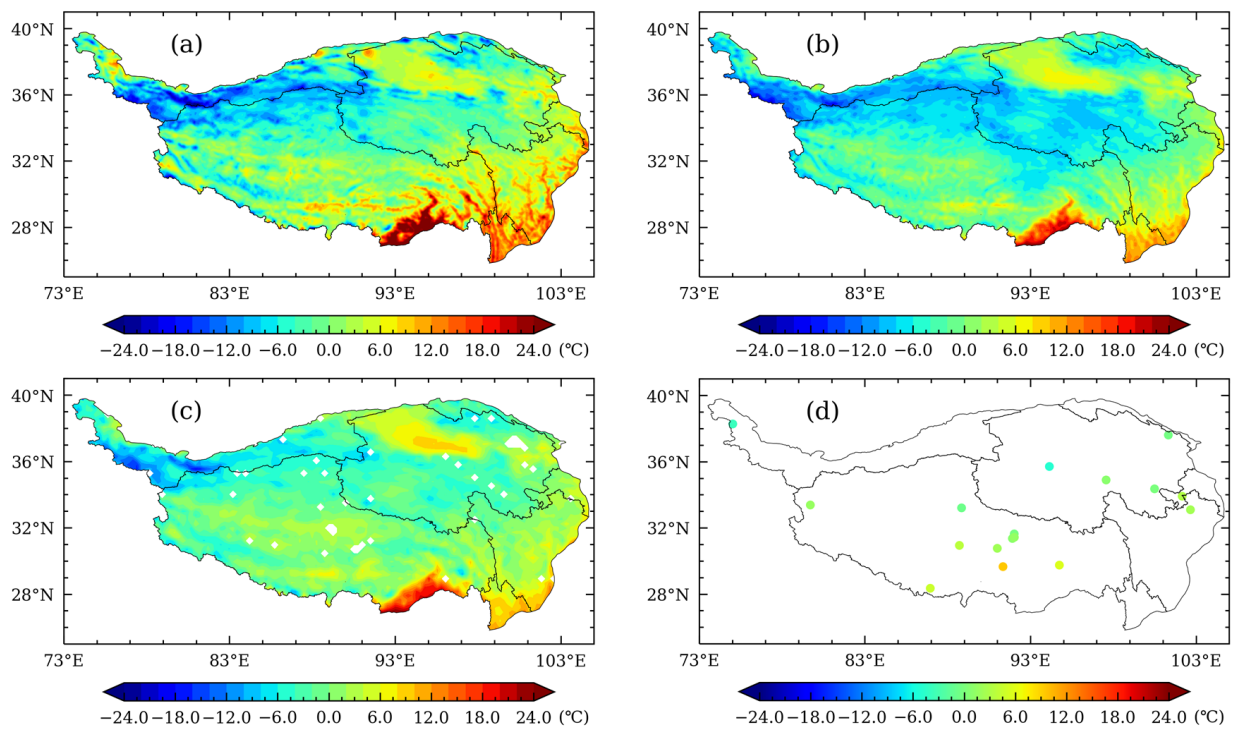


**Figure 5.** Spatial distributions of autumn mean temperature over 2017–2018 ((a) CLDAS; (b) ERA5L; (c) GLDAS; (d) in-situ observations).

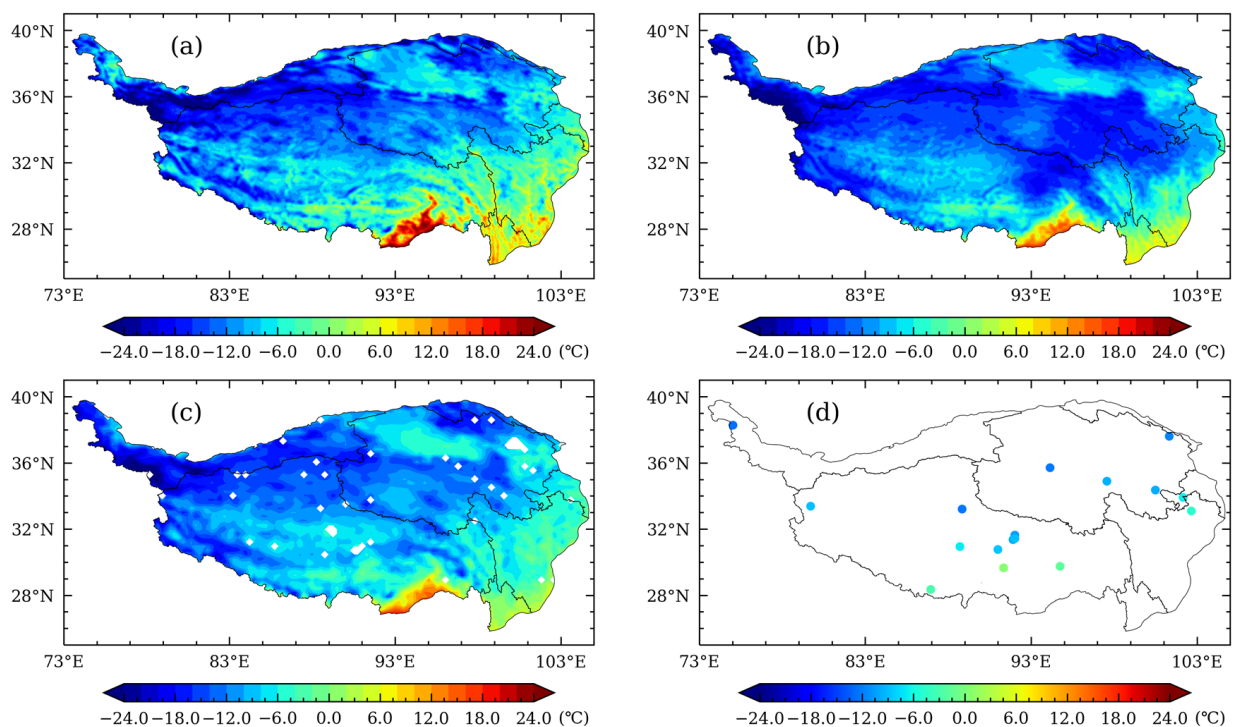


**Figure 6.** Spatial distributions of winter mean temperature over 2017–2018 ((a) CLDAS; (b) ERA5L; (c) GLDAS; (d) in-situ observations).

### 3.2. Accuracy of the Reanalysis Datasets for the Evaluation Period

Table 3 lists the evaluation results over the period 2017–2018. The mean temperatures of CLDAS, ERA5L, and GLDAS are 1.49 °C, −2.491 °C, and −0.44 °C, respectively. The mean value of CLDAS is the closest to the average of the in-situ observations (0.956 °C).

The correlation coefficient (CC) between CLDAS and the observations is the highest (0.969), followed by the correlation between ERA5L and the observations (0.934); the correlation coefficient between GLDAS and the observations is the lowest (0.92). The MBEs of ERA5L and GLDAS are  $-3.45\text{ }^{\circ}\text{C}$  and  $-1.40\text{ }^{\circ}\text{C}$ , respectively, which suggests that temperature is underestimated in the two reanalysis datasets, to a certain degree. Conversely, the MBE of CLDAS is 0.53, which indicates that CLDAS overestimates temperature in those in-situ observation sites. The RMSEs of CLDAS, ERA5L, and GLDAS are  $2.18\text{ }^{\circ}\text{C}$ ,  $4.83\text{ }^{\circ}\text{C}$ , and  $3.64\text{ }^{\circ}\text{C}$ , respectively, which indicates that the errors of CLDAS are smaller than the other two reanalyses. The values of NSE and WAI are close to 1 (the premium value) for all the three reanalysis datasets, suggesting that they are highly consistent with the in-situ observations, especially CLDAS. From the value of KGE, CLDAS is closer to 1, which indicates that it is better than ERA5L and GLDAS. This result agrees with NSE and WAI. In general, CLDAS is noticeably better than GDAS and ERA5L during the evaluation period based on evaluation indices of correlation, bias, and consistency. GLDAS is better than ERA5L, although the differences between them are relatively small.

**Table 3.** Accuracy evaluation results of CLDAS, ERA5L and GLDAS for the period 2017–2018.

Dataset	Mean Temperature ( $^{\circ}\text{C}$ )	CC	MBE ( $^{\circ}\text{C}$ )	RMSE ( $^{\circ}\text{C}$ )	NSE	KGE	WIA
CLDAS	1.49	0.969	0.534	2.175	0.933	0.44	0.983
ERA5L	-2.491	0.934	-3.447	4.827	0.67	-2.609	0.927
GLDAS	-0.44	0.92	-1.396	3.638	0.813	-0.463	0.952

To better display the consistency of the three reanalysis datasets with the observations during the evaluation period, Figure 7 shows the scatter plots of reanalysis data versus in-situ observations and the results of univariate linear regression. The goodness of fit ( $R^2$ ) for CLDAS, ERA5L, and GLDAS are 0.939, 0.872, and 0.847, respectively, which indicates that CLDAS is more consistent with in-situ observations. This result agrees with the results shown in Table 3.

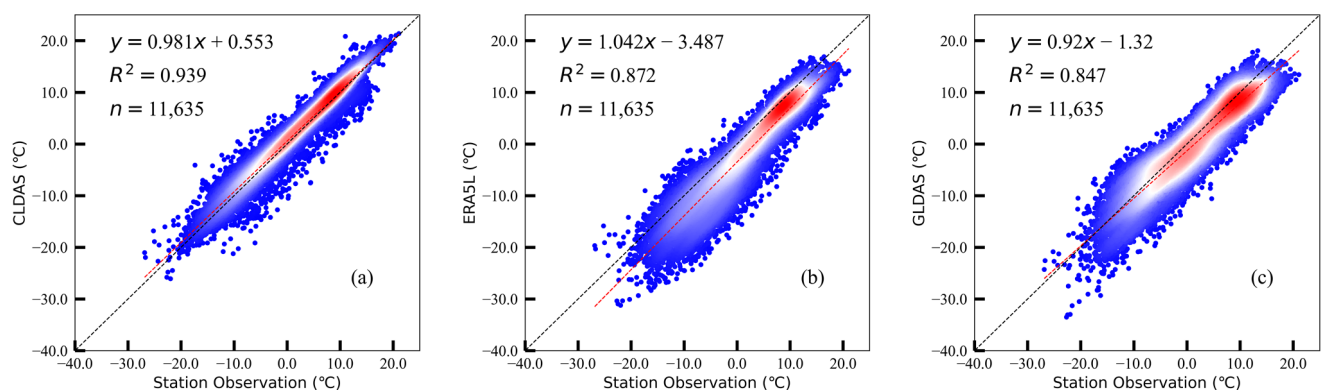


**Figure 7.** Scatter plots of reanalysis datasets versus in-situ observations ((a) CLDAS; (b) ERA5L; (c) GLDAS; n: total number of samples).

### 3.3. Evaluation of Temporal Variation

#### 3.3.1. Daily Variation

To analyze differences in daily temperature of the reanalysis datasets during the evaluation period, daily average temperatures of CLDAS, GLDAS, ERA5L, and in-situ observations over the evaluation period are displayed in Figure 8a, which shows that the daily variations and temporal changes of surface air temperature are basically consistent between the three reanalysis datasets and observations, and that CLDAS is closer to the observations than GLDAS and ERA5L are. Looking at the time series of daily CC (Figure 8b), we found that in 85.6% of the days, the CCs of CLDAS with observations are above 0.8.

However, the CCs of GLDAS and ERA5L with observations are below 0.8 in 60.7% and 90.5% of the days, respectively. Furthermore, the magnitude of daily variation of CLDAS is relatively small, which implies a more stable correlation with in-situ observations. The ranges of daily RMSE variation for CLDAS, ERA5L, and GLDAS (Figure 8c) are within 0.61–2.35 °C, 1.97–3.80 °C, and 2.43–3.76 °C, respectively. Note that the daily variation of RMSE for CLDAS is obviously lower than—the other two reanalysis datasets. In 76% of the total days, the RMSE values of GLDAS were lower than those of ERA5L, which indicates that the quality of GLDAS is higher than ERA5L in most days. The time series of daily MBE are displayed in Figure 8d, which shows that the MBEs of CLDAS are closer to the zero line than GLDAS and ERA5L are, which suggests that CLDAS is more consistent with observations than GLDAS and ERA5L. The MBE of CLDAS is positive in 78.5% of the days, whereas the MBE of GLDAS is negative in 90% of the days, and ERA5L is negative throughout the study period. This result indicates that daily temperature is overestimated by CLDAS and underestimated by GLDAS in most of the days, and it is always underestimated by ERA5L. The consistency indices of NSE (Figure 8e), KGE (Figure 8f), and WIA (Figure 8g) of CLDAS are closer to 1 with a smaller range of variation compared to that of ERA5L and GLDAS, which shows that CLDAS is more consistent with observations and demonstrates a higher stability.

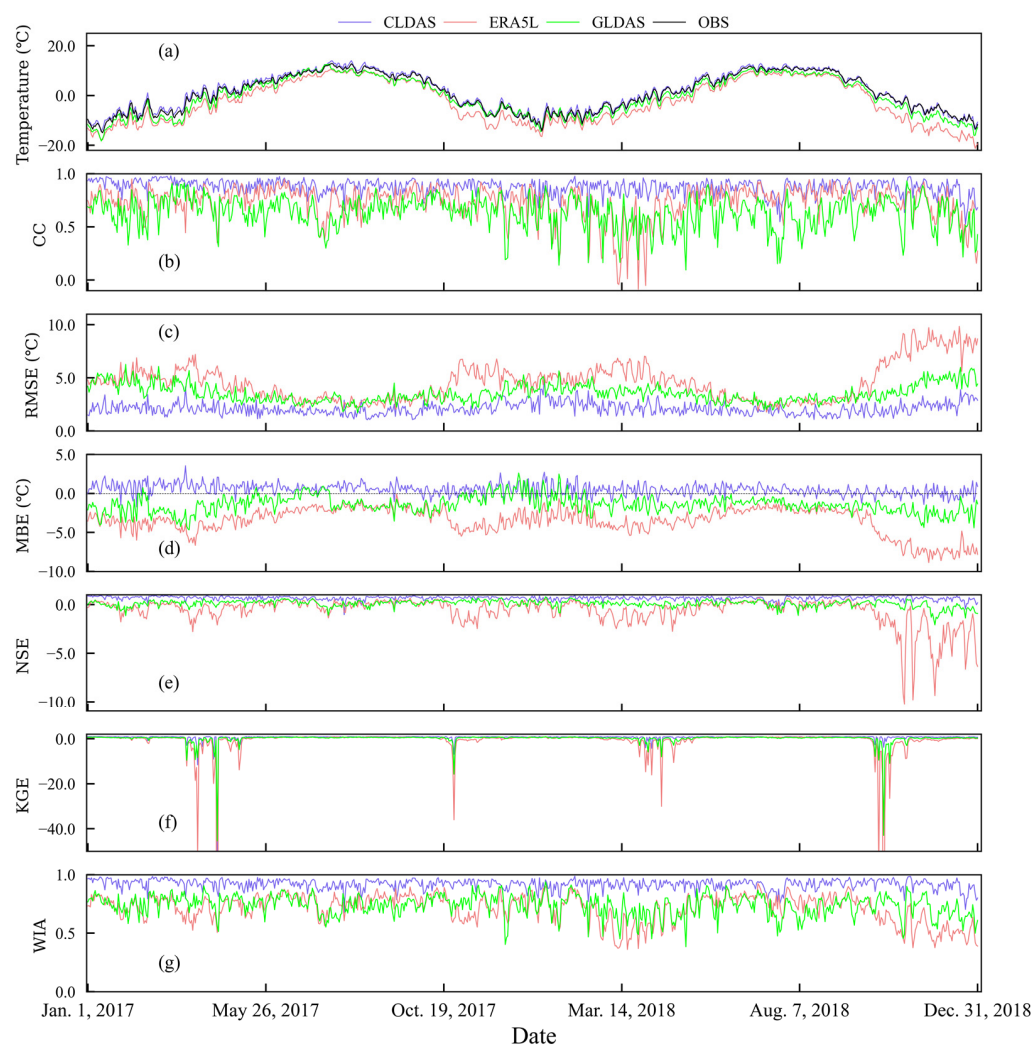


**Figure 8.** Daily evaluation of during 2017–2018. (a) Time series of daily mean temperature; (b) CC; (c) RMSE; (d) MBE; (e) NSE; (f) KGE; (g) WIA.

### 3.3.2. Monthly Variation

Figure 9 presents characteristic changes in monthly mean errors of the reanalysis datasets. The time series of monthly mean temperature (Figure 9a) indicates that the variation trends of the three reanalysis datasets are similar to that of the observations, i.e., temperature is the lowest in January and gradually increases from then onwards, reaches the highest in July, and then gradually decreases. Monthly CCs for CLDAS are all higher than those for GLDAS and ERA5L (Figure 9b). CCs for GLDAS are higher than for ERA5L in all months except March 2017 and February 2018, when the CCs for GLDAS are slightly lower than those of ERA5L. The RMSEs of CLDAS, ERA5L, and GLDAS (Figure 9c) range between 1.637–3.046 °C, 2.535–8.353 °C, and 2.682–5.054 °C, respectively. Note that the RMSEs of CLDAS are smaller than those of the DLDAS and ERA5L in all months, while the RMSEs of GLDAS are lower than those of ERA5L in all months except August and September of 2017 and July and August of 2018, when the RMSEs of GLDAS are slightly higher than those of ERA5L. Monthly MBE variations (Figure 9d) indicate that CLDAS overestimates monthly mean temperature in all months except December 2018, when it slightly underestimates the monthly mean temperature by  $-0.025$  °C. The largest overestimation of 1.172 °C occurs in March 2017. Monthly MBEs of ERA5L are negative in all months, with the largest negative bias of  $-7.395$  °C occurring in November 2018. Monthly MBEs of GLDAS are negative in all months except December 2017, when the monthly mean temperature of GLDAS is higher than the observation by 0.445 °C. The largest negative bias of GLDAS occurs in March 2017 with the value of  $-2.993$  °C. Monthly consistency indices of NSE (Figure 9e) for CLDAS, ERA5L, and GLDAS are within the ranges of 0.581–0.847,  $-2.253$ – $-0.363$ , and  $-0.191$ – $-0.541$ , respectively, and the ranges of KGE (Figure 9f) are 0.027–0.892,  $-26.714$ – $-0.736$ , and  $-8.948$ – $-0.709$ , respectively. The indices of WIA (Figure 9g) are within the ranges of 0.903–0.961, 0.545–0.855, and 0.685–0.865, respectively. The lowest value of NSE occurs in either July or August for all the three reanalysis datasets, whereas the lowest value of WIA occurs in either October or August. Compared to the other two reanalysis datasets, monthly values of NSE, KGE, and WIA for CLDAS are closer to one, suggesting that CLDAS is more consistent with observations. GLDAS overall is better than ERA5L, with the exception of a few months.

### 3.3.3. Seasonal Analysis

Figure 10 displays seasonal error characteristics during the evaluation period. The histograms of seasonal mean air temperature changes from reanalysis datasets and in-situ observations are displayed in Figure 10a, which shows that seasonal temperatures of CLDAS, ERA5L, and GLDAS as well as in-situ observations all present a unimodal feature of being low in winter and high in summer. This result indicates that the three reanalysis datasets can well describe the seasonal variation of temperature in the QTP. Seasonal CCs (Figure 10b) of the three reanalysis datasets with observations are all the highest in autumn, while the CCs of CLDAS and ERA5L with observations are the lowest in winter and higher in spring than in summer. Although the CC of GLDAS with observations is the lowest in summer, the difference between CCs in winter and summer is quite small. Seasonal RMSEs (Figure 10c) of the CLDAS, ERA5L, and GLDAS all gradually increase from the minimum values in summer (1.819 °C, 2.863 °C and 2.828 °C) to the maximum values in winter (2.62 °C, 5.693 °C and 4.451 °C), and then decrease in the spring. Seasonal MBEs are displayed in Figure 10d, which indicates that CLDAS overestimates seasonal mean temperature in all seasons, though the overestimation is relatively small in autumn. Opposite to CLDAS, ERA5L and GLDAS both underestimate seasonal mean temperature, and the underestimation is more severe in ERA5L. The largest negative bias occurs in autumn and the smallest negative bias occurs in summer for both ERA5L and GLDAS. The histograms of seasonal NSE (Figure 10e) and WIA (Figure 10g) show that the consistency of the three reanalysis data with in-situ observations is relatively poor in winter, and is optimal in autumn. However, from the perspective of KGE (Figure 10f), the three reanalysis datasets are worst in spring and better in summer.

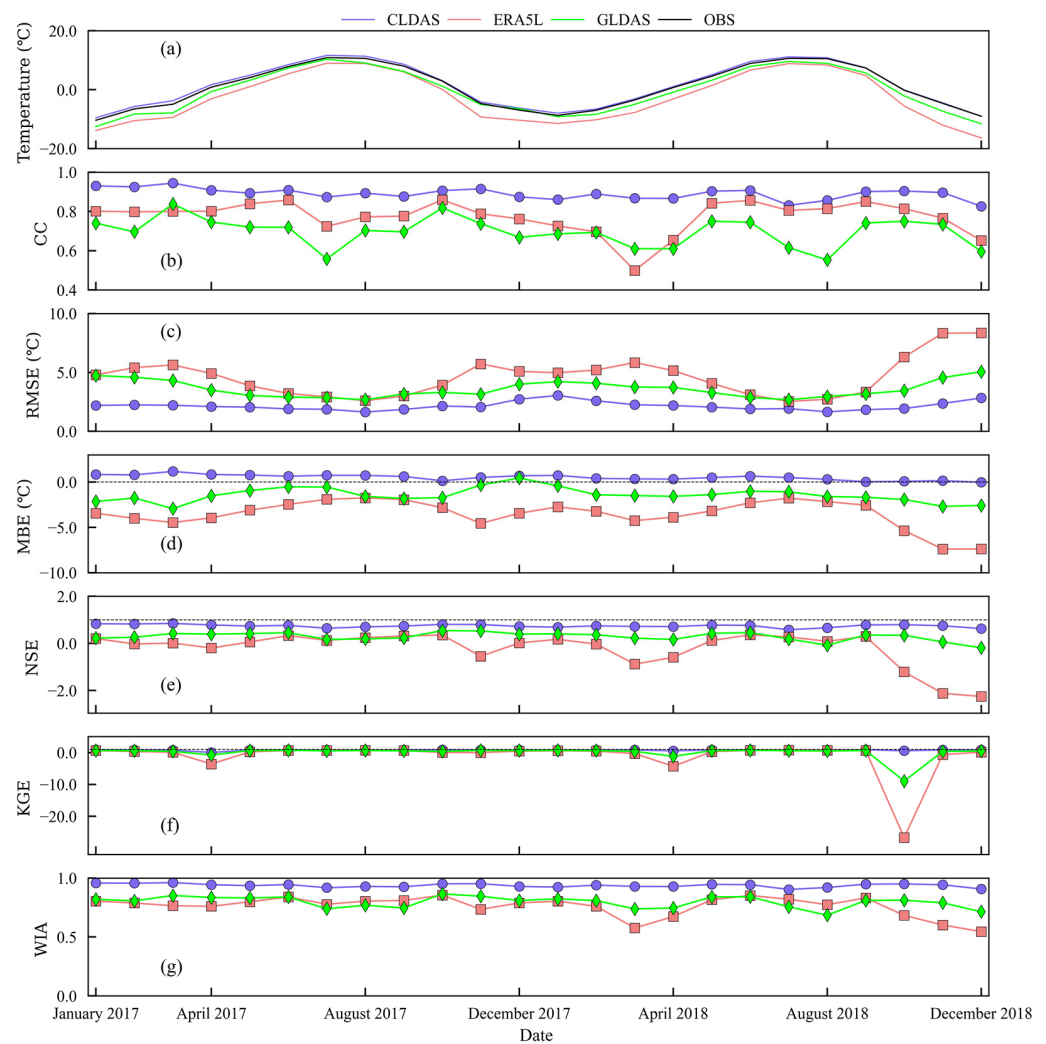


**Figure 9.** Monthly evaluation of during 2017–2018. (a): Series of monthly mean temperature; (b) CC; (c) RMSE; (d) MBE; (e) NSE; (f) NSE; (g) WIA.

### 3.4. Comparative Reanalysis at Individual Sites

Figure 11 shows box plots of temperature errors of CLDAS, GLDAS, and ERA5L during 2017–2018. The numbers of stations with CC (Figure 11a) higher than 0.95 account for 82.4%, 52.9%, and 70.6% of the total number of stations for CLDAS, ERA5L, and GLDAS, respectively. The lowest CCs, with respective values of 0.902, 0.915, and 0.913 for CLDAS, ERA5L, and GLDAS, all occur at Ruorgai (Elinghu), while the highest CCs occur at Ali and Golmud (0.992 for CLDAS), Haibei (0.974 for ERA5L), and Mushitage (0.979 for GLDAS). RMSEs (Figure 11b) are within the ranges of 1.222–4.289 °C, 2.345–6.076 °C, and 2.366–5.736 °C for CLDAS, ERA5L, and GLDAS, respectively. The largest RMSEs of CLDAS and ERA5L occur at Ruorgai (Elinghu), where the correlation is the lowest. The largest RMSE of GLDAS is found at Lasa. The smallest RMSEs of the three datasets occur at different sites. The box plot of MBE (Figure 11c) shows that CLDAS is lower than observations at only 4 sites, i.e., Ruorai (Elinghu), Sanjinagyuuan, Golmud, and Shenzha, which account for 23.5% of the total observation sites. The largest negative bias (−1.995) is found at Ruorgai (Elinghu), and the largest positive bias (1.99 °C) occurs at Naqu (Hanhansuo). ERA5L data are lower than observations at all sites, and the largest bias is found at Mushitage (−4.968 °C). Positive biases of GLDAS only occur at Ruorgai (Maqu), Naqu (Qingzangsu), Naqu (Hanhansuo), and Shuanghu, which account for 29.4% of the total stations. The largest positive bias occurs at Shuanghu (2.37 °C); the biases of GLDAS are negative at all other sites with the largest negative bias (−5.385 °C) at Lasa.

The consistency indices of NSE for CLDAS, ERA5L, and GLDAS (Figure 11d) are within the ranges of 0.748–0.974, 0.102–0.919, and 0.219–0.934, respectively, and the ranges of KGE (Figure 11e) are  $-157.108$ – $0.918$ ,  $-389.193$ – $0.537$ , and  $-138.881$ – $0.882$ , respectively. The ranges of WIA (Figure 11f) are 0.936–0.994, 0.85–0.978, and 0.839–0.982, respectively. Based on NSE, KGE, and WIA, the consistency of CLDAS is the worst at Ruoergai (Elinghu) and the consistency of GLDAS is the worst at Lasa. The consistency of ERA5L is worst at Zhufeng, Zangdongnan, and Lasa. In summary, the various reanalysis datasets show different qualities and applicability.

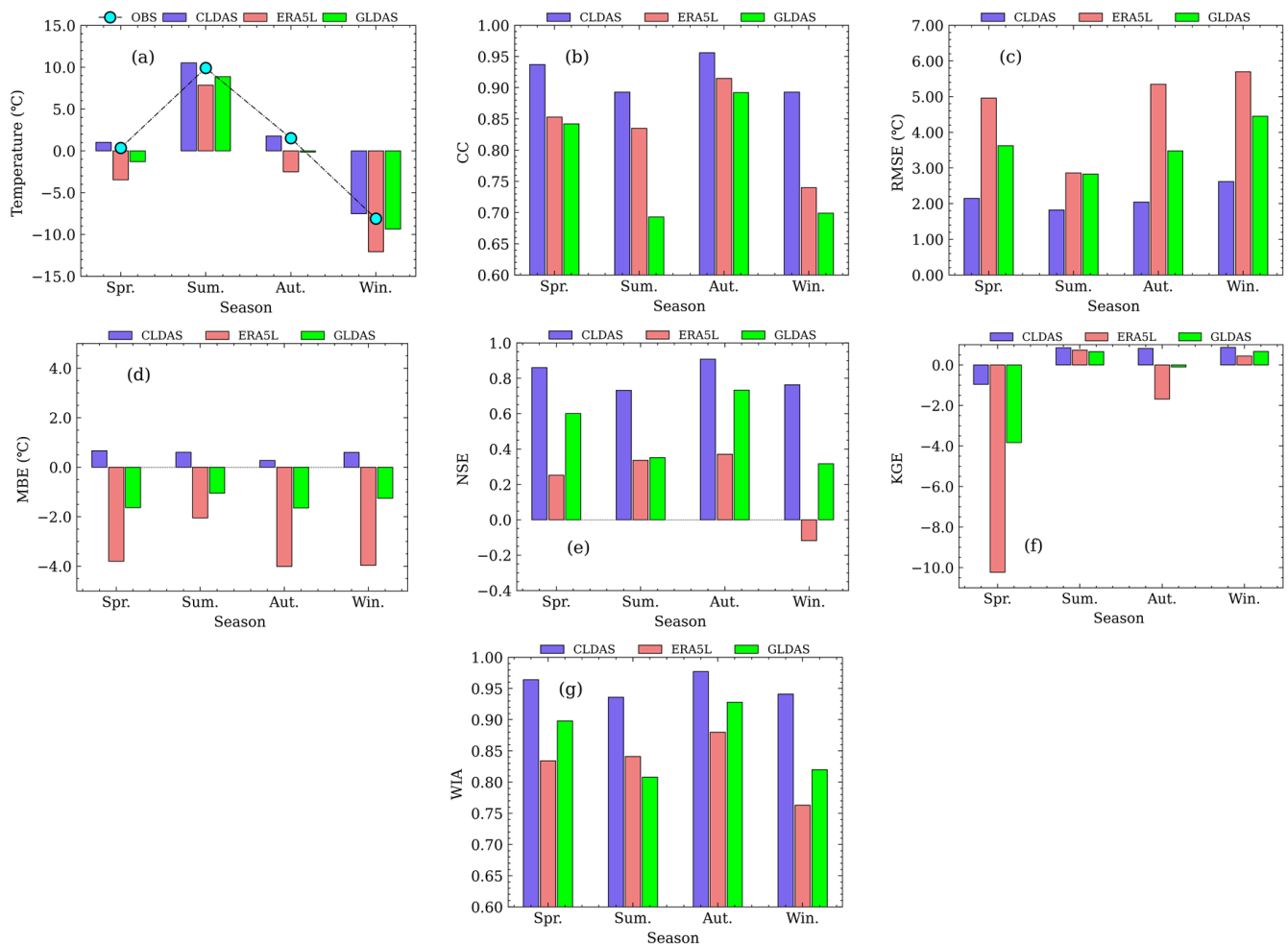


**Figure 10.** Seasonal evaluation during 2017–2018. (a): Seasonal changes of the average temperature; (b): CC; (c): RMSE; (d): MBE; (e): NSE; (f): KGE; (g): WIA.

To intuitively and easily understand the relationship between the consistency and errors of CLDAS, ERA5L, and GLDAS at the 17 observation stations, Taylor diagrams between the three reanalysis datasets and in-situ observations at each individual observation site are displayed in Figure 12. Figure 12a–q show that the standard deviations of CLDAS and GLDAS are relatively large at 11 and 7 sites, respectively, while ERA5L shows greater variability at 15 sites. The correlation coefficient between CLDAS and in-situ observations is larger than those between the other two reanalysis datasets and observations at all observation sites except Ruoergai (Elinghu), where the CC of CLDAS is slightly lower than the CC of GLDAS and ERA5L. The Taylor diagram between the three reanalysis datasets and all the in-situ observations (Figure 12r) indicates that CLDAS is closer to, and more consistent with, observations with smaller deviation.

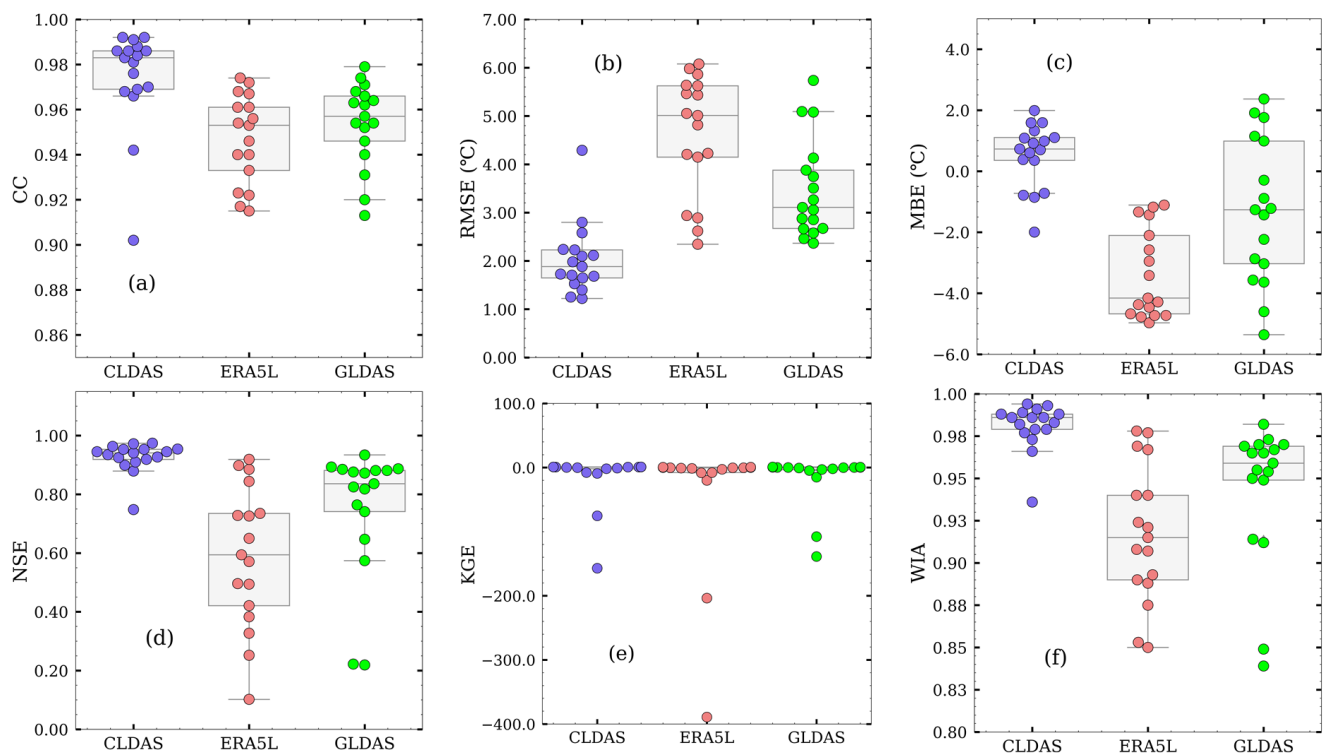


**Figure 11.** Box plots of temperature errors in CLDAS, ERA5L and GLDAS: (a) CC, (b) RMSE, (c) MBE, (d) NSE, (e) KGE, (f) WIA.

### 3.5. Comparative Reanalysis at Different Terrain Elevations

To explore the temperature variation characteristics of the three reanalysis datasets in different elevations, the observation sites are divided into four categories of elevation:  $<3500$  m,  $\geq 3500$ – $4000$  m,  $\geq 4000$ – $4500$  m, and  $\geq 4500$  m. Figure 13 show the bias characteristics of the three gridded datasets at different elevations. In terms of evaluation indices (CC, NSE, KGE, and WIA), the consistency between CLDAS and the in-station observations is higher than the other analysis products at any altitude. The MBEs of CLDAS show a positive deviation relative to the observation station, while ERA5L and GLDAS are opposite. The RMSEs of CLDAS are lower than those of the other two reanalysis datasets, and GLDAS is better than ERA5L. Although the CCs of ERA5L is slightly higher than GLDAS, other indices (NSE, KGE and WIA) are relatively lower than GLDAS. Compared to ERA5L and GLDAS, the CLDAS temperature data is less affected by elevation.

### 3.6. Comparative Reanalysis at Different Land Covers

According to the land cover type, the observation sites are divided into seven categories: alpine meadow (AE), desert (DT), grassland in forests (GF), gravel (GL), peatland (PD), sand and gravel (SG), and artificial grassland (AG). Figure 14 show the bias characteristics of CLDAS, ERA5L, and GLDAS at different land covers. The MBEs of ERA5L and GLDAS showed negative deviation in in-station observations at different land covers, while CLDAS is opposite. The deviation of CLDAS at land cover of artificial grassland is the smallest, as are ERA5L and GLDAS with alpine meadow and peatland, respectively. In essence, the consistency indices (CC, NSE, KGE, and WIA) and deviation (MBE and RMSE) between CLDAS and in-station observations have a small range of variation, and are better than ERA5L and GLDAS in each land cover.

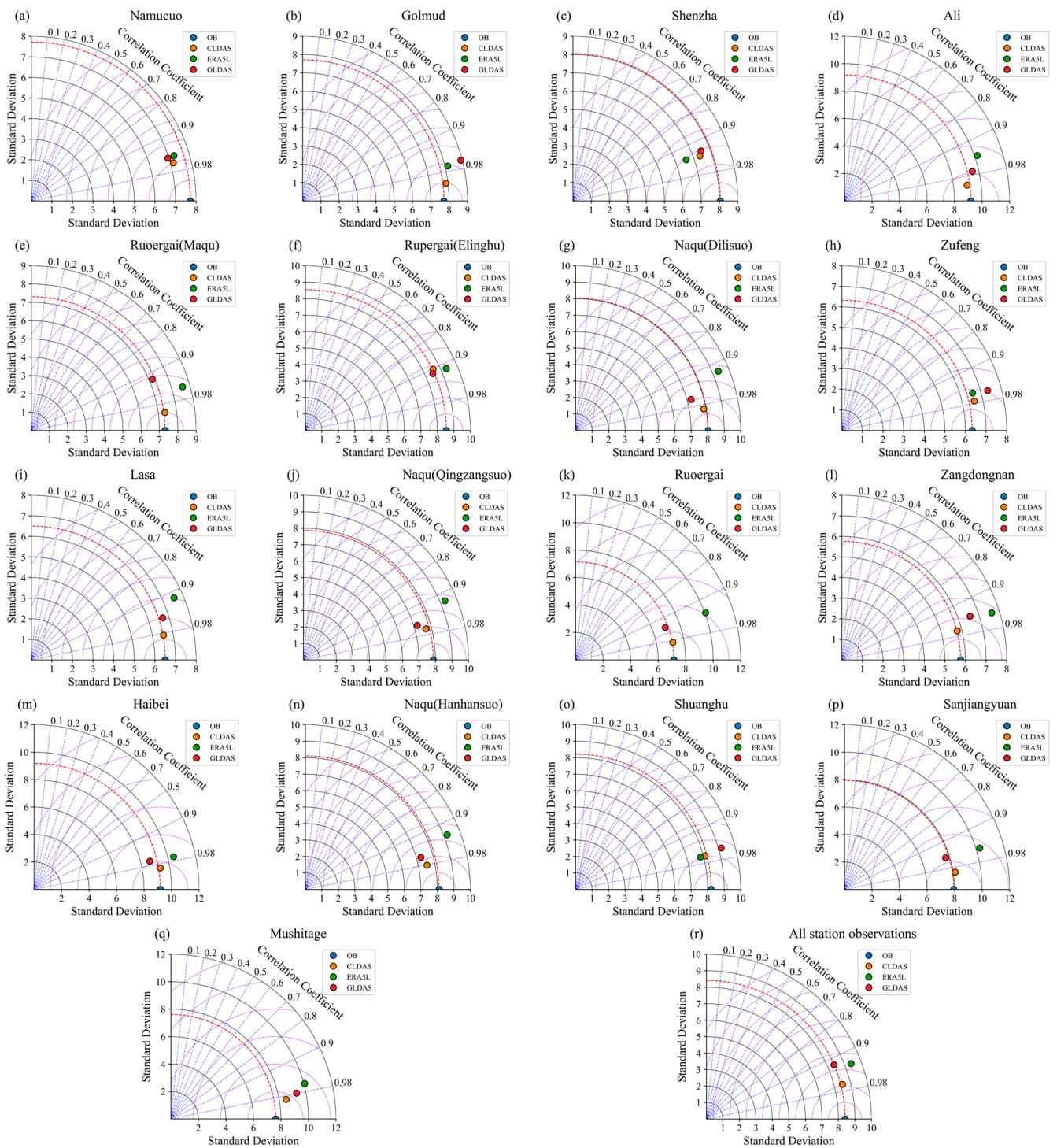


Figure 12. Taylor diagrams of (a–q) CLDAS, ERA5L, GLDAS against in-situ observations at 17 stations and (r) all observation stations.

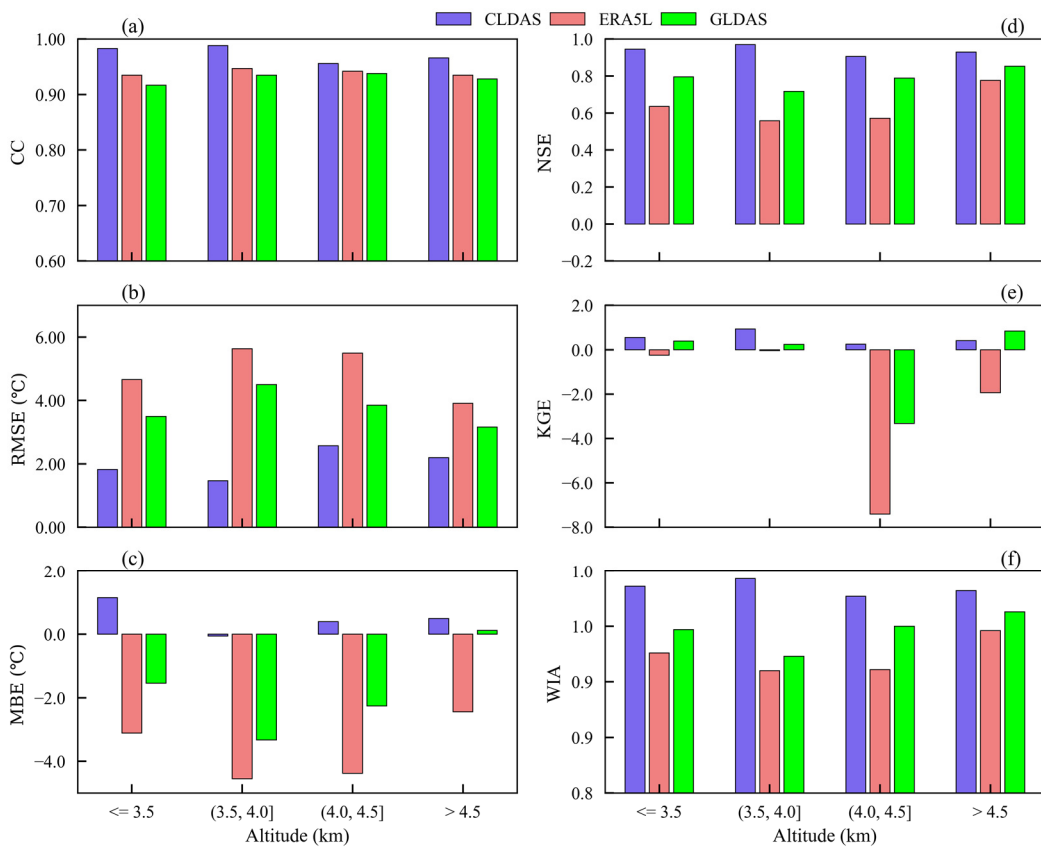


Figure 13. The errors at different altitudes: (a) CC; (b) RMSE; (c) MBE; (d) NSE; (e) KGE; (f) WIA.

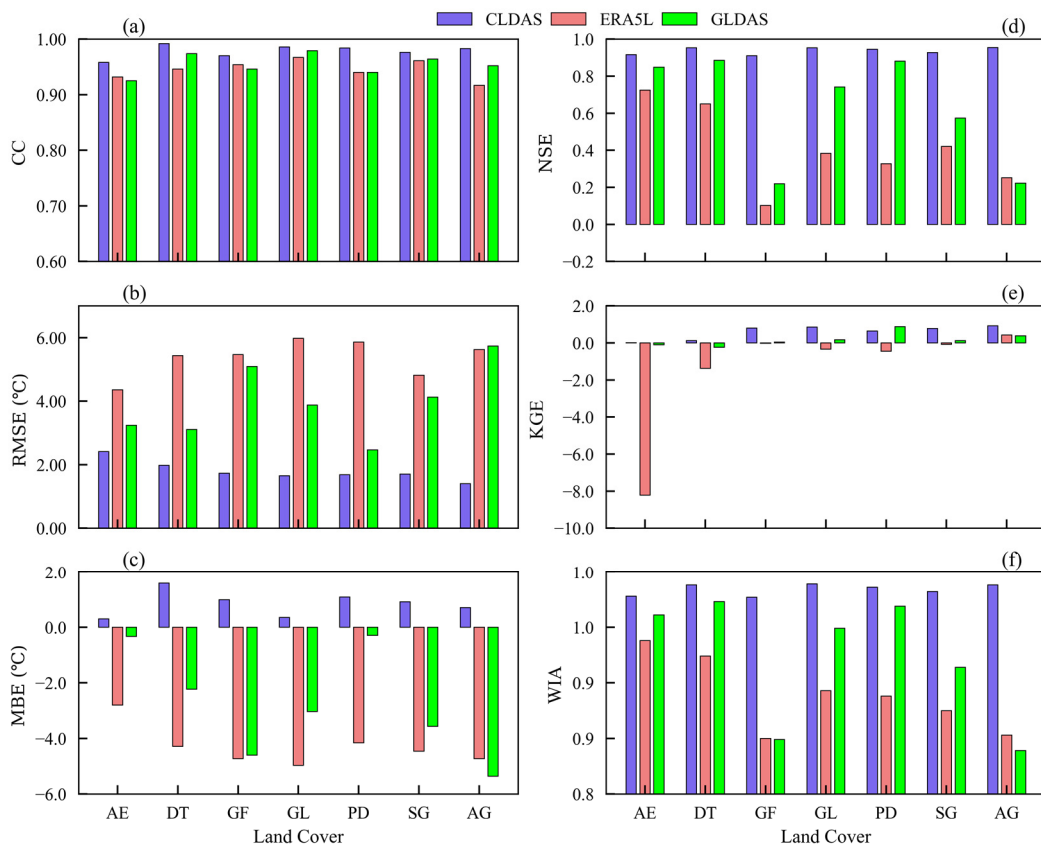


Figure 14. The errors at different land covers: (a) CC; (b) RMSE; (c) MBE; (d) NSE; (e) KGE; (f) WIA.

#### 4. Discussion

Based on the validation results, we found that a certain degree of errors are inevitable in the three reanalysis datasets in comparison to in-situ observations. Surface air temperature in the QTP is not only controlled by regional factors (longitude, latitude), but also affected by other factors such as geographical conditions (altitude, aspect, slope) and the underlying surface (such as vegetation, snow cover), and are further complicated by temperature changes [55–63].

Several previous studies have also found differences of biases between stations and air temperature reanalysis datasets. For example, Huang et al. [41] found that elevation is not the only factor that causes biases in reanalysis datasets. Through the assessment of the slopes of in-situ observation sites, they found that the errors and applicability of CLDAS, ERA5L, and GLDAS increase with the increasing slope of the observation site. Ding et al. [64] found that temperature changes are significantly correlated with the elevation and slope of the observation site, and the complexity of the terrain is the main factor leading to large errors in reanalysis data. Meanwhile, these results also indicate that when using temperature reanalysis data, topographic correction should be performed on the data in order to effectively reduce errors and improve the accuracy and applicability of the reanalysis data. Liu and Long et al. [42,65] evaluated CLDAS; Huang et al. [41] evaluated CLDAS, ERA5L, and GLDAS in China. They found that that the errors of the three reanalysis datasets all increase with increasing monthly average temperatures, and the correlation between the reanalysis data and the in-situ observations gradually decreased, reaching the minimum value in July or August. The correlation and bias then gradually increased with decreasing temperature. However, the present study indicates that the monthly variation of errors in the QTP is not significant, though the seasonal variation is essentially the same with the previous studies of Huang et al. [41], which may be attributed to the differences in the time series of the data used and the division of regions.

Errors that resulted from the approach of evaluation at individual sites can be influenced by a few factors: (1) The spatial scales do not match. The in-situ observations at a specific site only reflect temperature changes in a certain area around it, and, due to the influence of topography, the representativeness of the observations is still limited. In contrast, the reanalysis data at a specific grid represents the average value of the grid. Thus, it is difficult to solve the problem of spatial mismatch [56,59] between in-situ observations and gridded reanalysis data. (2) The difference between the terrain height of the re-analysis grid and the elevation of the station [41,42,66]. If the observation site is located in a valley and its altitude is lower than the altitude of the surrounding grid points of the reanalysis dataset, the evaluation result at this site will generally show a colder deviation; if the site is located at the top of mountains, which is higher than the elevation of the surrounding grids in the reanalysis dataset, the evaluation result will show a warm bias at this site. (3) Systematic errors [67,68] caused by the numerical model or assimilation method. For example, cold errors occur at 70.6% and 100% of the total number of stations for GLDAS and ERA5L, respectively, which may be caused by systematic errors. In addition, errors in input data and errors introduced during the interpolation of reanalysis data (e.g., from Gaussian grids to coordinate grids) are also sources of errors that need to be further verified. Therefore, error characteristics and the applicability of reanalysis data should be fully considered in the application of temperature reanalysis data. Next, we will resample the three reanalysis datasets at the same resolution and use different interpolation methods for evaluation to discuss the influences on the accuracy of the gridded datasets.

##### 4.1. Impact of Grid Resolutions on the Accuracy of the Reanalysis Datasets

To explore the temperature variation characteristics and accuracy of the three reanalysis datasets at the same resolution, GLDAS and ERA5L are resampled to GLDAS grids with the spatial resolution of  $0.25^\circ$  using the mean value algorithm [55], and thus the three reanalysis datasets have uniform temporal and spatial resolutions. Figure 15 show the spatial distributions of annual mean temperature over 2017–2018. Although remapping

CLDAS and ERA5L reduces the resolution, it still shows more advantages in detail than GLDAS. Figure 16 shows the bias of annual mean temperature between in-situ observations and reanalysis datasets at 17 weather stations. It is easy to find that, at each observation station, CLDAS has a small deviation to in-situ observations compared with ERA5L and GLDAS.

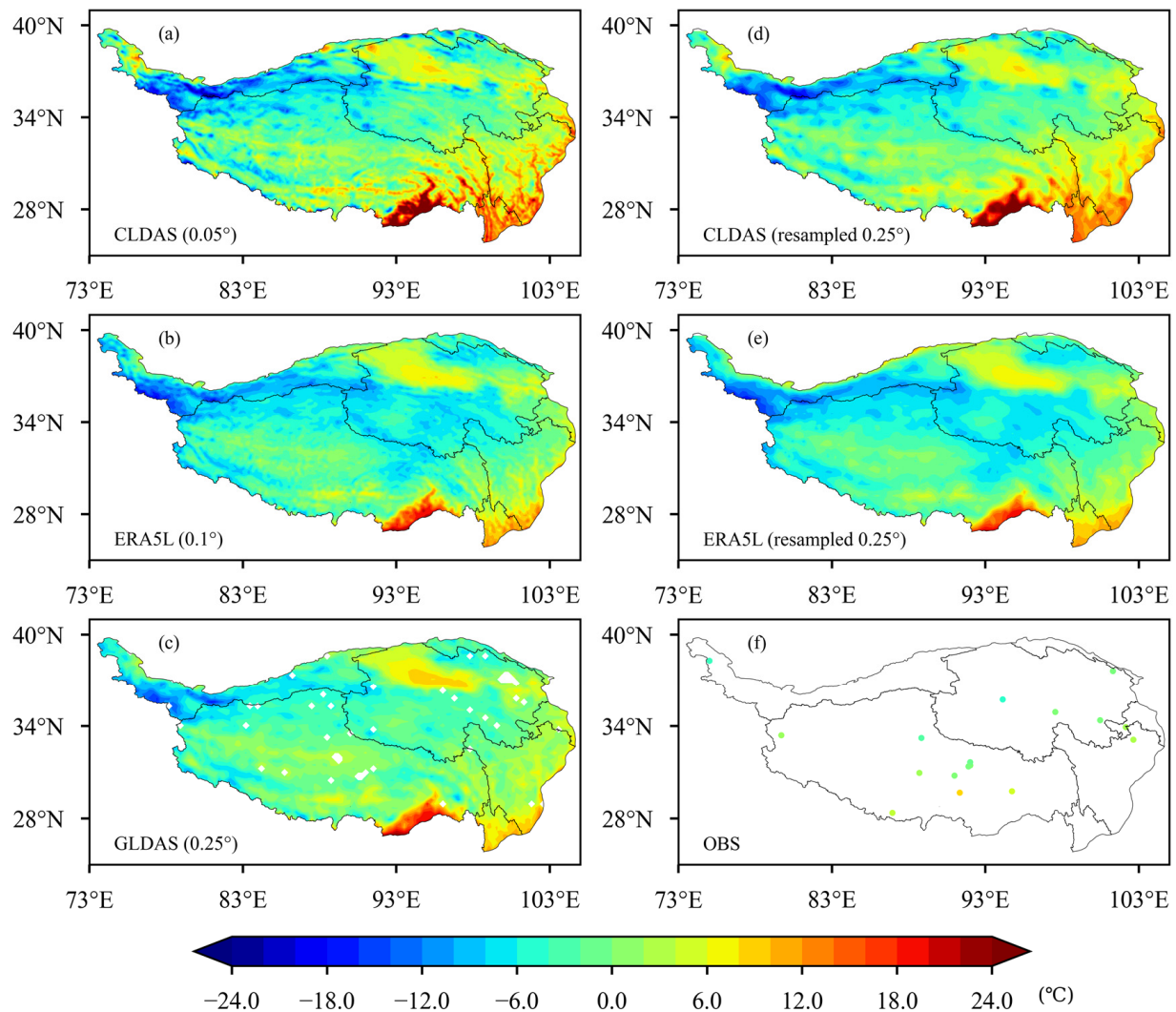


**Figure 15.** Spatial distributions of annual mean temperature over 2017–2018. (a) CLDAS (0.05°); (b) ERA5L (0.1°); (c) CLDAS (0.25°); (d) CLDAS (resampled to 0.25°); (e) ERA5L (resampled to 0.25°); (f) OBS (in-situ observations).

#### 4.2. Impact of Interpolation Methods on the Accuracy of the Reanalysis Datasets

In order to analyze the impact of different interpolation methods on the evaluation results, the two most common interpolation methods, nearest neighbor method and bilinear interpolation method, are used in the present study [40,42]. The results are shown in Table 4. We found that different interpolation methods can have a certain impact on the evaluation results, but the impact is very small. It can also be seen that the bilinear interpolation method also shows that the deviation of CLDAS from the in-situ observations is lower than the other two reanalysis datasets, and that GLDAS is better than ERA5L.

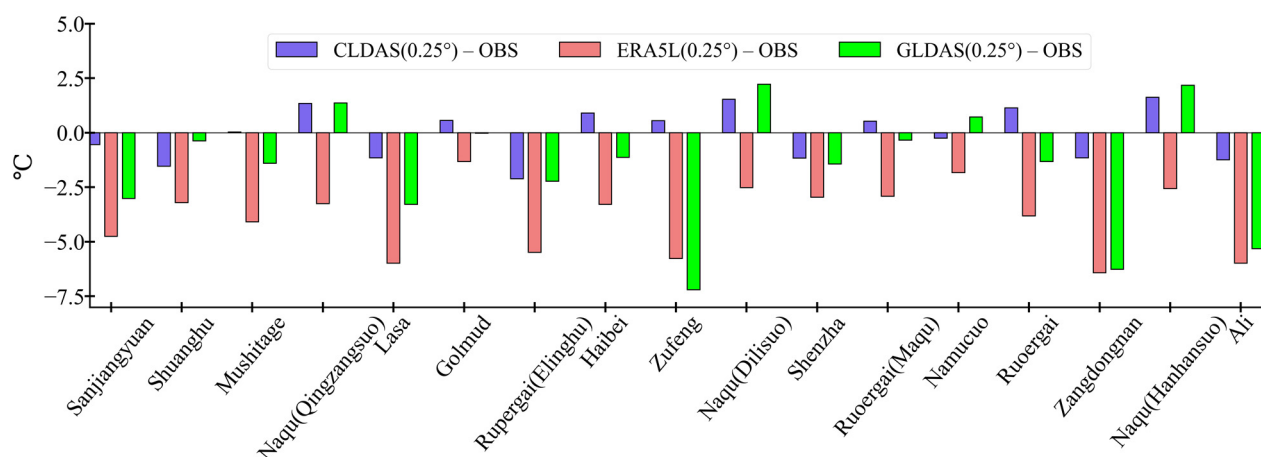


**Figure 16.** The bias of annual mean temperature between in-situ observations (OBS) and three reanalysis datasets over 2017–2018.

**Table 4.** Accuracy evaluation results used two interpolation methods for the evaluation period.

Dataset	CC		MBE (°C)		RMSE (°C)		NSE		KGE		WIA	
	Nea	Bil	Nea	Bil	Nea	Bil	Nea	Bil	Nea	Bil	Nea	Bil
CLDAS	0.969	0.968	0.534	0.404	2.175	2.179	0.933	0.933	0.44	0.576	0.983	0.983
ERA5L	0.934	0.933	−3.447	−3.61	4.827	4.942	0.67	0.654	−2.609	−2.779	0.927	0.924
GLDAS	0.92	0.927	−1.396	−1.103	3.638	3.37	0.813	0.839	−0.463	−0.157	0.952	0.958

Note: Nearest neighbor interpolation method (Nea), bilinear interpolation method (Bil).

Although all three reanalysis datasets can accurately reflect the distribution characteristics of air temperature in the alpine region of the QTP, CLDAS performs better overall. It is also better at individual stations and on daily, monthly, and seasonal time scales. One important reason is that in the QTP, CLDAS integrates the observations collected at thousands of surface automatic weather stations [22,35], which is of great benefit to the quality of CLDAS. ERA5L and GLDAS are global reanalysis products, both of which show large deviations from observations, probably due to the lack of observations for assimilation over the QTP. Furthermore, when compared with the other two reanalysis datasets, CLDAS also has higher spatial resolution, which can improve its ability for temperature description [40], especially in complex terrain areas. Using data assimilation and fusion techniques with in-situ observation data, satellite remote sensing data, and numerical model data, the reanalysis system produces regular gridded data with a certain temporal and spatial resolution. This process will introduce some uncertainties [22] into the final data products, which is why deviation of reanalysis from in-situ observations is important.

Based on the aforementioned discussion, we believe that, although there are certain deviations in the temperature reanalysis datasets in the QTP, they still have certain applicability and credibility in the alpine region of the QTP, where observation sites are unevenly distributed with a low density of observations. Thus, these reanalysis datasets have certain reference values. It should be noted that, even though the quality of CLDAS is better than the other two datasets based on careful evaluation of the three reanalysis datasets in the present study, the reanalysis datasets of ERA5L and GLDAS have longer time sequences, larger spatial coverage, and better continuity compared to CLDAS. Due to the extremely complex terrain in the QTP and the short sequences of in-situ observations at the 17 sites, which cannot cover all of the QTP area, the three datasets have their respective advantages and disadvantages in different areas and further studies are necessary for local scale.

## 5. Conclusions

In this study, the consistency between in-situ observations collected at 17 field observation stations in the alpine region of the QTP and the three reanalysis datasets (CLDAS, GLDAS, and ERA5L) and their deviations from observations from 2017–2018 are evaluated. Major conclusions are as follows:

- (1) The spatial distributions of the three reanalysis datasets and the in-situ observations follow the change patterns of latitude and elevation. Temporal variations of average temperature and spatial distributions of temperature in the reanalysis datasets, as well as their correlations with and deviation from in-situ observations, all indicate that the three reanalysis datasets are consistent with observations and demonstrate reasonability. Despite some slight differences in local or regional scales, the magnitudes of the data and their spatial distributions remain consistent.
- (2) The spatial distributions of the three reanalysis datasets are consistent, while CLDAS is closer to, and more consistent with, observations than GLDAS and ERA5L are. In the spring, CLDAS temperature is higher than ERA5L and GLDAS over the entire study area except the Qaidam Basin and the low elevation area of southern Tibet. Compared to ERA5L and GLDAS, CLDAS shows smaller differences in spatial distribution. In the summer, spatial distributions of CLDAS and GLDAS are closer, while ERA5L is obviously lower. In the autumn, CLDAS and ERA5L become closer, while GLDAS is relatively low in the high-elevation area of the western QTP but relatively high in the low-elevation area of the southeastern QTP. In the winter, ERA5L is lower than CLDAS and GLDAS in southeastern Qinghai and northeastern Tibet.
- (3) Evaluation results on multi-time scales (daily, monthly, and seasonal) and multi-space scales (individual stations, elevations, and land covers) indicate that the accuracy and applicability of CLDAS are discernibly better than the other two datasets. GLDAS is better than ERA5L, but the difference between the two is small. However, the quality of the reanalysis datasets is different at observation sites.

In summary, CLDAS is more consistent with observations than GLDAS and ERA5L are and demonstrates better capability for the description of temperature in the alpine region of the QTP. Despite certain defects and limitations, ERA5L and GLDAS are still reliable and applicable in the alpine area of the QTP where observations are sparse and unevenly distributed. Results of the present paper have great implications for ecosystems and sustainable development studies in the QTP.

**Author Contributions:** Conceptualization, X.H., S.H. and C.S.; methodology, X.H., S.H. and C.S.; validation, S.H.; data curation, S.H. and C.S.; writing—original draft preparation, X.H.; writing—review and editing, X.H., S.H. and C.S.; visualization, X.H.; supervision, S.H.; funding acquisition, S.H. and C.S. All authors have read and agreed to the published version of the manuscript.

**Funding:** This research was funded by the National Key Research and Development Program of China (No. 2018YFC1506601), the Key Research and Development Program of Sichuan (No. 2022YFS0541), the Key Techniques and Data Sets of Land Surface Reanalysis in Qinghai Xizang Plateau (No. NMICJY202106), Study on the Fusion of Precipitation and Soil Moisture with Multi-Source Data (No. 2011DFG23150), and the Innovative Development Project of the China Meteorological Administration (No. CXFZ2021Z007).

**Acknowledgments:** The authors appreciate the National Tibetan Plateau Data Center for providing the meteorological observation data set of HORN in 2017–2018, and thank all the participants in the field observations. We are very grateful for the helpful input and suggestions from the anonymous reviewers and editors.

**Conflicts of Interest:** The authors declare no conflict of interest.

## References

1. Qiu, J. China: The third pole. *Nature* **2008**, *454*, 393–397. [[CrossRef](#)] [[PubMed](#)]
2. Wu, G.; Liu, Y.; Zhang, Q.; Duan, A.; Wang, T.; Wan, R.; Liu, X.; Li, W.; Wang, Z.; Liang, X. The influence of mechanical and thermal forcing by the Tibetan Plateau on Asian climate. *J. Hydrometeorol.* **2007**, *8*, 770–789. (In Chinese) [[CrossRef](#)]
3. Xu, X.; Dong, L.; Zhao, Y.; Wang, Y. Effect of the Asian Water Tower over the Qinghai-Tibet Plateau and the characteristics of atmospheric water circulation. *Chin. Sci. Bull.* **2019**, *64*, 2830–2841. [[CrossRef](#)]
4. Deliang, C.; Baiqing, X.; Tandong, Y.; ZhengTang, G.; Peng, C.; FaHu, C.; Zhang, R.; Zhang, X.; Zhang, Y.; Jie, F. Assessment of past, present and future environmental changes on the Tibetan Plateau. *Chin. Sci. Bull.* **2015**, *60*, 3025–3035. (In Chinese) [[CrossRef](#)]
5. Ma, Y.; Hu, Z.; Tian, L.; Zhang, F.; Duan, A.; Yang, K.; Zhang, Y.; Yang, Y. Study progresses of the Tibet Plateau climate system change and mechanism of its impact on East Asia. *Adv. Earth Sci.* **2014**, *29*, 207–215. (In Chinese) [[CrossRef](#)]
6. Zhang, R.; Fengge, S.; Jiang, Z.; Xuejie, G.; Donglin, G.; Jian, N.; Qinglong, Y.; Cuo, L.; BoTao, Z. An overview of projected climate and environmental changes across the Tibetan Plateau in the 21st century. *Chin. Sci. Bull.* **2015**, *60*, 3036–3047. (In Chinese) [[CrossRef](#)]
7. Yao, T.; Yu, W.; Wu, G.; Xu, B.; Yang, W.; Zhao, H.; Wang, W.; Li, S.; Wang, N.; Li, Z. Glacier anomalies and relevant disaster risks on the Tibetan Plateau and surroundings. *Chin. Sci. Bull.* **2019**, *64*, 2770–2782. (In Chinese) [[CrossRef](#)]
8. Sheridan, S.C.; Lee, C.C.; Smith, E.T. A comparison between station observations and reanalysis data in the identification of extreme temperature events. *Geophys. Res. Lett.* **2020**, *47*, e2020GL088120. [[CrossRef](#)]
9. Tandong, Y.; Shilong, P.; Miaogen, S.; Jing, G.; Wei, Y.; Guoqing, Z.; Yanbin, L.; Yang, G.; Liping, Z.; Baiqing, X. Chained impacts on modern environment of interaction between Westerlies and Indian Monsoon on Tibetan Plateau. *Bull. Chin. Acad. Sci.* **2017**, *32*, 976–984. (In Chinese) [[CrossRef](#)]
10. Fu, Y.; Ma, Y.; Zhong, L.; Yang, Y.; Guo, X.; Wang, C.; Xu, X.; Yang, K.; Xu, X.; Liu, L. Land-surface processes and summer-cloud-precipitation characteristics in the Tibetan Plateau and their effects on downstream weather: A review and perspective. *Natl. Sci. Rev.* **2020**, *7*, 500–515. [[CrossRef](#)]
11. DingYihui, Z. Intercomparison of the time for climate abrupt change between the Tibetan Plateau and other regions in China. *Chin. J. Atmos. Sci.* **2008**, *32*, 794–805. (In Chinese)
12. Liu, X.; Chen, B. Climatic warming in the Tibetan Plateau during recent decades. *Int. J. Climatol.* **2000**, *20*, 1729–1742. [[CrossRef](#)]
13. Hansen, J.; Ruedy, R.; Sato, M.; Lo, K. Global surface temperature change. *Rev. Geophys.* **2010**, *48*, RG4004. [[CrossRef](#)]
14. You, Q.; Kang, S.; Chen, D.; Li, J.; Ji, Z. Several research frontiers of climate change over the Tibetan Plateau. *J. Glaciol. Geocryol.* **2021**, *43*, 885–901. (In Chinese) [[CrossRef](#)]
15. Duo, C.; Yong, Y.; Jiancan, L.; Ciren, B. Applicability analysis of MERRA surface air temperature over the Qinghai-Xizang Plateau. *Plateau Meteorol.* **2016**, *35*, 337–350. (In Chinese) [[CrossRef](#)]
16. Wang, X.; Pang, G.; Yang, M. Precipitation over the Tibetan Plateau during recent decades: A review based on observations and simulations. *Int. J. Climatol.* **2018**, *38*, 1116–1131. [[CrossRef](#)]
17. Zhao, T.; Fu, C. Applicability evaluation of surface air temperature from several reanalysis datasets in China. *Plateau Meteorol.* **2009**, *28*, 594–606. (In Chinese)
18. Zheng, R.; Li, D.; Jiang, Y. New characteristics of temperature change over Qinghai-Xizang Plateau on the background of global warming. *Plateau Meteorol.* **2015**, *34*, 1531–1539. (In Chinese) [[CrossRef](#)]
19. Han, S.; Shi, C.; Sun, S.; Gu, J.; Xu, B.; Liao, Z.; Zhang, Y.; Xu, Y. Development and Evaluation of a Real-Time Hourly One-Kilometre Gridded Multisource Fusion Air Temperature Dataset in China Based on Remote Sensing DEM. *Remote Sens.* **2022**, *14*, 2480. [[CrossRef](#)]
20. Gao, K.; Duan, A.; Chen, D.; Wu, G. Surface energy budget diagnosis reveals possible mechanism for the different warming rate among Earth's three poles in recent decades. *Sci. Bull.* **2019**, *64*, 1140–1143. [[CrossRef](#)]
21. Lai, H.-W.; Chen, H.W.; Kukulies, J.; Ou, T.; Chen, D. Regionalization of seasonal precipitation over the Tibetan Plateau and associated large-scale atmospheric systems. *J. Clim.* **2021**, *34*, 2635–2651. [[CrossRef](#)]
22. Shi, C.; Pan, Y.; Gu, J.; Xu, B.; Han, S.; Zhu, Z.; Zhang, L.; Sun, S.; Jiang, Z. A review of multi-source meteorological data fusion products. *Acta Meteorol. Sin.* **2019**, *77*, 774–783. (In Chinese) [[CrossRef](#)]
23. Xia, Y.; Hao, Z.; Shi, C.; Li, Y.; Meng, J.; Xu, T.; Wu, X.; Zhang, B. Regional and global land data assimilation systems: Innovations, challenges, and prospects. *J. Meteorol. Res.* **2019**, *33*, 159–189. [[CrossRef](#)]
24. Jiang, Y.; Han, S.; Shi, C.; Gao, T.; Zhen, H.; Liu, X. Evaluation of HRCLDAS and ERA5 Datasets for Near-Surface Wind over Hainan Island and South China Sea. *Atmosphere* **2021**, *12*, 766. [[CrossRef](#)]
25. Hersbach, H.; Bell, B.; Berrisford, P.; Horányi, A.; Sabater, J.M.; Nicolas, J.; Radu, R.; Schepers, D.; Simmons, A.; Soci, C. Global reanalysis: Goodbye ERA-Interim, hello ERA5. *ECMWF Newsl.* **2019**, *159*, 17–24.
26. Hersbach, H.; Bell, B.; Berrisford, P.; Hirahara, S.; Horányi, A.; Muñoz-Sabater, J.; Nicolas, J.; Peubey, C.; Radu, R.; Schepers, D. The ERA5 global reanalysis. *Q. J. R. Meteorol. Soc.* **2020**, *146*, 1999–2049. [[CrossRef](#)]
27. Hoffmann, L.; Günther, G.; Li, D.; Stein, O.; Wu, X.; Griessbach, S.; Heng, Y.; Konopka, P.; Müller, R.; Vogel, B. From ERA-Interim to ERA5: The considerable impact of ECMWF's next-generation reanalysis on Lagrangian transport simulations. *Atmos. Chem. Phys.* **2019**, *19*, 3097–3124. [[CrossRef](#)]

28. Muñoz-Sabater, J.; Dutra, E.; Agustí-Panareda, A.; Albergel, C.; Arduini, G.; Balsamo, G.; Boussetta, S.; Choulga, M.; Harrigan, S.; Hersbach, H. ERA5-Land: A state-of-the-art global reanalysis dataset for land applications. *Earth Syst. Sci. Data Discuss.* **2021**, *13*, 4349–4383. [[CrossRef](#)]
29. Xu, W.; Lei, X.; Chen, S.; Zhang, M.; Jiang, L.; Bao, R.; Guan, X.; Ma, M.; Wei, J.; Feng, A. How well does the ERA5 reanalysis capture the extreme climate events over China? Part II: Extreme temperature. *Front. Environ. Sci.* **2022**, *10*, 756. [[CrossRef](#)]
30. Pelosi, A.; Terribile, F.; D’Urso, G.; Chirico, G.B. Comparison of ERA5-Land and UERRA MESCAN-SURFEX reanalysis data with spatially interpolated weather observations for the regional assessment of reference evapotranspiration. *Water* **2020**, *12*, 1669. [[CrossRef](#)]
31. Ghazanfari, S.; Pande, S.; Hashemy, M.; Sonneveld, B. Diagnosis of GLDAS LSM based aridity index and dryland identification. *J. Environ. Manag.* **2013**, *119*, 162–172. [[CrossRef](#)] [[PubMed](#)]
32. Rodell, M.; Houser, P.; Jambor, U.; Gottschalck, J.; Mitchell, K.; Meng, C.-J.; Arsenault, K.; Cosgrove, B.; Radakovich, J.; Bosilovich, M. The global land data assimilation system. *Bull. Am. Meteorol. Soc.* **2004**, *85*, 381–394. [[CrossRef](#)]
33. Wu, Z.; Feng, H.; He, H.; Zhou, J.; Zhang, Y. Evaluation of Soil Moisture Climatology and Anomaly Components Derived from ERA5-Land and GLDAS-2.1 in China. *Water Resour. Manag.* **2021**, *35*, 629–643. [[CrossRef](#)]
34. Shi, C.; Xie, Z.; Qian, H.; Liang, M.; Yang, X. China land soil moisture EnKF data assimilation based on satellite remote sensing data. *Sci. China Earth Sci.* **2011**, *54*, 1430–1440. [[CrossRef](#)]
35. Han, S.; Shi, C.; Jiang, Z.; Xu, B.; Li, X.; Zhang, T.; Jiang, L.; Liang, X.; Zhu, Z.; Liu, J. Development and progress of high resolution CMA land surface data assimilation system. *Adv. Meteorol. Sci. Technol.* **2018**, *8*, 102–108 + 116. (In Chinese) [[CrossRef](#)]
36. Sun, S.; Shi, C.; Pan, Y.; Bai, L.; Xu, B.; Zhang, T.; Han, S.; Jiang, L. Applicability assessment of the 1998–2018 CLDAS multi-source precipitation fusion dataset over China. *J. Meteorol. Res.* **2020**, *34*, 879–892. [[CrossRef](#)]
37. Wang, Q.; Li, W.; Xiao, C.; Ai, W. Evaluation of High-Resolution Crop Model Meteorological Forcing Datasets at Regional Scale: Air Temperature and Precipitation over Major Land Areas of China. *Atmosphere* **2020**, *11*, 1011. [[CrossRef](#)]
38. Han, S.; Shi, C.; Xu, B.; Sun, S.; Zhang, T.; Jiang, L.; Liang, X. Development and Evaluation of Hourly and Kilometer Resolution Retrospective and Real-Time Surface Meteorological Blended Forcing Dataset(SMBFD) in China. *J. Meteorol. Res.* **2019**, *33*, 1168–1181. [[CrossRef](#)]
39. Liu, L.; Gu, H.; Xie, J.; Xu, Y.P. How well do the ERA-Interim, ERA-5, GLDAS-2.1 and NCEP-R2 reanalysis datasets represent daily air temperature over the Tibetan Plateau? *Int. J. Climatol.* **2021**, *41*, 1484–1505. [[CrossRef](#)]
40. Han, S.; Liu, B.; Shi, C.; Liu, Y.; Qiu, M.; Sun, S. Evaluation of CLDAS and GLDAS datasets for Near-surface Air Temperature over major land areas of China. *Sustainability* **2020**, *12*, 4311. [[CrossRef](#)]
41. Huang, X.; Han, S.; Shi, C. Multiscale Assessments of Three Reanalysis Temperature Data Systems over China. *Agriculture* **2021**, *11*, 1292. [[CrossRef](#)]
42. Liu, Y.; Shi, C.; Wang, H.; Han, S. Applicability assessment of CLDAS temperature data in China. *Trans. Atmos. Sci.* **2021**, *44*, 540–548. (In Chinese) [[CrossRef](#)]
43. Wang, W.; Gao, Y.; Xu, J. Applicability of GLDAS and climate change in the Qinghai-Xizang Plateau and its surrounding arid area. *Plateau Meteorol.* **2013**, *32*, 635–645. (In Chinese) [[CrossRef](#)]
44. Peng, P.; Zhu, L. Observations of land surface processes of the Tibetan Plateau based on the field stations network. *Sci. Technol. Rev.* **2017**, *35*, 97–102. (In Chinese) [[CrossRef](#)]
45. Peng, P.; Zhu, L. *Meteorological Data of Surface Environment and Observation Network in China’s Cold Region (2018)*; National Tibetan Plateau Data Center: Beijing, China, 2020. [[CrossRef](#)]
46. Rolland, C. Spatial and seasonal variations of air temperature lapse rates in Alpine regions. *J. Clim.* **2003**, *16*, 1032–1046. [[CrossRef](#)]
47. Camargo, L.R.; Schmidt, J. Simulation of multi-annual time series of solar photovoltaic power: Is the ERA5-land reanalysis the next big step? *Sustain. Energy Technol. Assess.* **2020**, *42*, 100829. [[CrossRef](#)]
48. Wang, W.; Cui, W.; Wang, X.; Chen, X. Evaluation of GLDAS-1 and GLDAS-2 forcing data and Noah model simulations over China at the monthly scale. *J. Hydrometeorol.* **2016**, *17*, 2815–2833. [[CrossRef](#)]
49. Rui, H.; Beaudoin, H. README Document for NASA GLDAS Version 2 Data Products. Available online: [https://hydro1.gesdisc.eosdis.nasa.gov/data/GLDAS/README\\_GLDAS2.pdf](https://hydro1.gesdisc.eosdis.nasa.gov/data/GLDAS/README_GLDAS2.pdf) (accessed on 10 July 2022).
50. Nash, J.E.; Sutcliffe, J.V. River flow forecasting through conceptual models part I—A discussion of principles. *J. Hydrol.* **1970**, *10*, 282–290. [[CrossRef](#)]
51. Moriasi, D.N.; Arnold, J.G.; Van Liew, M.W.; Bingner, R.L.; Harmel, R.D.; Veith, T.L. Model evaluation guidelines for systematic quantification of accuracy in watershed simulations. *Trans. ASABE* **2007**, *50*, 885–900. [[CrossRef](#)]
52. Gupta, H.V.; Kling, H.; Yilmaz, K.K.; Martinez, G.F. Decomposition of the mean squared error and NSE performance criteria: Implications for improving hydrological modelling. *J. Hydrol.* **2009**, *377*, 80–91. [[CrossRef](#)]
53. Pool, S.; Vis, M.; Seibert, J. Evaluating model performance: Towards a non-parametric variant of the Kling-Gupta efficiency. *Hydrol. Sci. J.* **2018**, *63*, 1941–1953. [[CrossRef](#)]
54. Willmott, C.J. On the validation of models. *Phys. Geogr.* **1981**, *2*, 184–194. [[CrossRef](#)]
55. Ji, L.; Senay, G.B.; Verdin, J.P.J.o.H. Evaluation of the Global Land Data Assimilation System (GLDAS) air temperature data products. *J. Hydrometeorol.* **2015**, *16*, 2463–2480. [[CrossRef](#)]
56. You, Q.; Fraedrich, K.; Ren, G.; Pepin, N.; Kang, S. Variability of temperature in the Tibetan Plateau based on homogenized surface stations and reanalysis data. *Int. J. Climatol.* **2013**, *33*, 1337–1347. [[CrossRef](#)]

57. You, Q.; Kang, S.; Pepin, N.; Flügel, W.-A.; Yan, Y.; Behrawan, H.; Huang, J. Relationship between temperature trend magnitude, elevation and mean temperature in the Tibetan Plateau from homogenized surface stations and reanalysis data. *Glob. Planet. Chang.* **2010**, *71*, 124–133. [[CrossRef](#)]
58. Li, X.; Cheng, G.; Lu, L. Spatial analysis of air temperature in the Qinghai-Tibet Plateau. *Arct. Antarct. Alp. Res.* **2005**, *37*, 246–252. [[CrossRef](#)]
59. Yang, J.; Huang, M.; Zhai, P. Performance of the CRA-40/Land, CMFD, and ERA-Interim datasets in reflecting changes in surface air temperature over the Tibetan Plateau. *J. Meteorol. Res.* **2021**, *35*, 663–672. [[CrossRef](#)]
60. Yin, H.; Sun, Y.; Donat, M.G. Changes in temperature extremes on the Tibetan Plateau and their attribution. *Environ. Res. Lett.* **2019**, *14*, 124015. [[CrossRef](#)]
61. Ding, L.; Zhou, J.; Zhang, X.; Liu, S.; Cao, R. Downscaling of surface air temperature over the Tibetan Plateau based on DEM. *Int. J. Appl. Earth Obs. Geoinf.* **2018**, *73*, 136–147. [[CrossRef](#)]
62. Hu, G.; Zhao, L.; Wu, X.; Li, R.; Wu, T.; Su, Y.; Hao, J.J.T.; Climatology, A. Evaluation of reanalysis air temperature products in permafrost regions on the Qinghai-Tibetan Plateau. *Theor. Appl. Climatol.* **2019**, *138*, 1457–1470. [[CrossRef](#)]
63. Peng, X.; Frauenfeld, O.W.; Jin, H.; Du, R.; Qiao, L.; Zhao, Y.; Mu, C.; Zhang, T. Assessment of temperature changes on the Tibetan Plateau during 1980–2018. *Earth Space Sci.* **2021**, *8*, e2020EA001609. [[CrossRef](#)]
64. Ding, M.; Du, J.; Xiao, T. Applicability of the four reanalysis temperature data in Chang Tang Nature Reserve. *J. Glaciol. Geocryol.* **2020**, *42*, 1046–1056. (In Chinese) [[CrossRef](#)]
65. Long, K.; Shi, C.; Han, S.; Huang, X.; Xu, X.; Sun, S.; Gu, J. Quality assessment of High Resolution Temperature Merged Grid Analysis Product in China. *Plateau Mt. Meteorol. Res.* **2019**, *39*, 67–74. (In Chinese) [[CrossRef](#)]
66. Shi, G.; Sun, Z.; Qiu, X.; Zeng, Y.; Chen, P.; Liu, C. Comparison of two air temperature gridding methods over complex terrain in China. *Theor. Appl. Climatol.* **2018**, *133*, 1009–1019. [[CrossRef](#)]
67. Gao, L.; Bernhardt, M.; Schulz, K. Elevation correction of ERA-Interim temperature data in complex terrain. *Hydrol. Earth Syst. Sci.* **2012**, *16*, 4661–4673. [[CrossRef](#)]
68. Wang, A.; Zeng, X. Evaluation of multireanalysis products with in situ observations over the Tibetan Plateau. *J. Geophys. Res. Atmos.* **2012**, *117*, d05102. [[CrossRef](#)]